

Polarization-dependent magnetic properties of periodically driven α -RuCl₃Naoya Arakawa^{1,*} and Kenji Yonemitsu^{1,2}¹*The Institute of Science and Engineering, Chuo University, Bunkyo, Tokyo 112-8551, Japan*²*Department of Physics, Chuo University, Bunkyo, Tokyo 112-8551, Japan*

(Received 1 July 2021; revised 31 August 2021; accepted 17 November 2021; published 8 December 2021)

We study magnetic properties of a periodically driven Mott insulator with strong spin-orbit coupling and show some properties characteristic of linearly polarized light. We consider a t_{2g} -orbital Hubbard model driven by circularly or linearly polarized light with strong spin-orbit coupling and derive its effective Hamiltonian in the strong-interaction limit for a high-frequency case. We show that linearly polarized light can change not only the magnitudes and signs of the exchange interactions, but also their bond anisotropy even without the bond-anisotropic hopping integrals. Because of this property, the honeycomb-network spin system could be transformed into weakly coupled zigzag or step spin chains for the light field polarized along the b or a axis, respectively. Then, analyzing how the light fields affect several magnetic states in a mean-field approximation, we show that linearly polarized light can change the relative stability of the competing magnetic states, whereas such a change is absent for circularly polarized light. We also analyze the effects of both the bond anisotropy of nearest-neighbor hopping integrals and a third-neighbor hopping integral on the magnetic states and show that the results obtained in a simple model, in which the bond-averaged nearest-neighbor hopping integrals are considered, remain qualitatively unchanged except for the stability of zigzag states in the nondriven case and the degeneracy lifting of the zigzag or stripy states.

DOI: [10.1103/PhysRevB.104.214413](https://doi.org/10.1103/PhysRevB.104.214413)**I. INTRODUCTION**

In periodically driven systems, magnetic properties can be controlled via a time-periodic field. In the presence of a time-periodic field, the solution to the Schrödinger equation satisfies the Floquet theorem and the Floquet Hamiltonian, a time-independent Hamiltonian, can describe the time evolution in steps of the driving period T [1–3]. Such a description may be appropriate if the effects of heating due to the driving field are negligible; such a situation could be realized before the system approaches an infinite-temperature state [4,5]. Since the Floquet Hamiltonian usually depends on parameters of the driving field, it is possible to control magnetic properties of a periodically driven system. For example, in a single-orbital Mott insulator driven by $E(t) = E_0 \cos \omega t$, we can change the magnitude and sign of the antiferromagnetic Heisenberg interaction by tuning E_0 and ω [6]. This or an extended method could be used to control magnetic properties of Mott insulators.

If a periodically driven Mott insulator has strong spin-orbit coupling (SOC), it may offer possibility for controlling various exchange interactions and magnetic states. The low-energy excitations of a Mott insulator with strong SOC can be described by the spin and orbital entangled degrees of freedom [7–9] and its effective Hamiltonian has not only the Heisenberg interaction, but also the anisotropic exchange interactions [10–14]. Then, various magnetic states appear, depending on the values of the Heisenberg interaction and the anisotropic exchange interactions [12,13,15–19]. In our

previous paper [20], we showed that by applying a circularly polarized light field $\mathbf{E}(t) = (E_0 \cos \omega t, -E_0 \sin \omega t)$ to a multi-orbital Mott insulator with strong SOC and tuning ω and E_0 , the magnitudes and signs of three exchange interactions can be changed simultaneously; these interactions are the Heisenberg interaction J , the Kitaev interaction K , and the off-diagonal symmetric exchange interaction Γ .

The aim of this paper is to clarify the polarization dependences of magnetic properties for a periodically driven Mott insulator with strong SOC. First, it is essential to understand the similarities and differences between the effects of circularly and linearly polarized light. In general, magnetic properties of solids depend on the polarization of light [21]. It is also necessary to clarify how the changes in exchange interactions due to a light field affect energies of several magnetic states. These topics are not discussed in our previous paper [20].

In this paper, we study the exchange interactions and the energies of several magnetic states for a periodically driven Mott insulator with strong SOC. We consider a t_{2g} -orbital Hubbard model on the honeycomb lattice with strong SOC and a field of linearly or circularly polarized light as a model of periodically driven α -RuCl₃. To analyze the effects of both the bond anisotropy of nearest-neighbor hopping integrals and a third-neighbor hopping integral, we consider five cases of our model, including a simple case considered in our previous paper [20]; the differences among them are about the hopping integrals. Treating the effects of one of the light fields as Peierls phase factors and using the Floquet theory [6,20,22], we derive the effective Hamiltonian of periodically driven α -RuCl₃ in the strong-interaction limit for a high-frequency case. Evaluating the exchange interactions numerically in the first two cases of our model, we show that linearly polarized

*arakawa@phys.chuo-u.ac.jp

light can be used to change not only the magnitudes and signs of J , K , and Γ , but also their bond anisotropy even without the bond anisotropy of the hopping integrals. This property, which is distinct from the effects of circularly polarized light [20], could be used to transform the honeycomb-network spin system into weakly coupled zigzag or step spin chains. We also show that the effects of the bond anisotropy of the nearest-neighbor hopping integrals are just quantitative in the sense that it only induces weak bond anisotropy of the exchange interactions. Then, by using a mean-field approximation (MFA), we evaluate the expectation value of our effective Hamiltonian. Analyzing the effects of the light fields on the energies of several magnetic states in the five cases of our model, we show that linearly polarized light can change the relative stability of the competing magnetic states, whereas circularly polarized light does not. Furthermore, we show that the results obtained in the simple case remain qualitatively unchanged except that the stability of the zigzag states or the ferromagnetic state depends on the strength of the bond anisotropy of the hopping integrals and the value of the third-neighbor hopping integral and that the degeneracy of the zigzag or stripy states is lifted not only by the fields of linearly polarized light, but also by the bond anisotropy of the hopping integrals.

The rest of the paper is organized as follows. In Sec. II, we introduce the Hamiltonian of our model. It consists of the hopping integrals of the t_{2g} -orbital electrons on the honeycomb lattice with a light field $\mathbf{E}(t)$, their LS coupling, and the t_{2g} -orbital Hubbard interactions. There are three $\mathbf{E}(t)$'s considered: $\mathbf{E}_{\text{circ}}(t)$, $\mathbf{E}_{\text{linear-}b}(t)$, and $\mathbf{E}_{\text{linear-}a}(t)$ [Eqs. (2)–(4)]. We consider five cases of our model, one of which is used in our previous paper [20]; the others are used to study the effects of the bond-anisotropic nearest-neighbor hopping integrals and the third-neighbor hopping integral. In Sec. III A, we express the effective Hamiltonian of our periodically driven Mott insulator in terms of the isotropic and the anisotropic exchange interactions. In Sec. III B, we present the $|u_{ij}| (= eE_0/\omega)$ dependences of the exchange interactions estimated numerically in the first two cases of our model. We compare the results for the three $\mathbf{E}(t)$'s and discuss the properties characteristic of the linearly polarized light. In Sec. IV A, by applying the MFA to our effective Hamiltonian, we derive an expression of the energy of a magnetic state characterized by the ordering vector. We also explain the characteristics of the magnetic states considered. In Sec. IV B, we present the $|u_{ij}|$ dependences of the numerically evaluated energies of several magnetic states in the five cases of our model. Comparing the results for the three $\mathbf{E}(t)$'s, we discuss the similarities and differences between the effects of the fields of circularly and linearly polarized light. We also analyze how the bond anisotropy of the nearest-neighbor hopping integrals and the third-neighbor hopping integral affect the magnetic states. In Sec. V, we discuss the validity of our model, the effects of heating, and an experimental observation of our results. Furthermore, we remark on a property induced by a field of circularly polarized light and several directions for further relevant research. In Sec. VI, we summarize the main results and their implications.

Throughout this paper, we set $\hbar = 1$ and $a_{\text{NN}} = 1$, where a_{NN} denotes the distance between nearest-neighbor sites on the honeycomb lattice (Fig. 1). This choice of a_{NN} leads

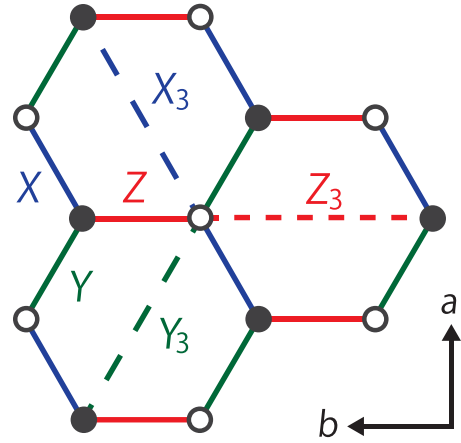


FIG. 1. Structure of the honeycomb lattice. Blue, green, and red lines represent three nearest-neighbor bonds, i.e., X , Y , and Z bonds, respectively; blue, green, and red dashed lines represent three third-neighbor bonds, i.e., X_3 , Y_3 , and Z_3 bonds, respectively. Black and white circles denote the A and B sublattices, respectively. This sublattice structure is necessary because the honeycomb lattice, which is not a Bravais lattice, can be represented as a triangular Bravais lattice with a two-point basis [23]. The a and b axes of the crystal are also shown.

to $a_{2\text{nd}} = \sqrt{3}$ and $a_{3\text{rd}} = 2$, where $a_{2\text{nd}}$ and $a_{3\text{rd}}$ denote the distances between second-neighbor and third-neighbor, respectively, sites. For simplicity, we neglect a small difference between the lengths of a Z bond and of an X or Y bond.

II. MODEL

Our model Hamiltonian consists of three parts:

$$H = H_{\text{KE}} + H_{\text{SOC}} + H_{\text{int}}, \quad (1)$$

where H_{KE} represents the kinetic energy, H_{SOC} represents the atomic SOC [8], and H_{int} represents the Coulomb interactions [24].

The kinetic energy is given by the hopping integrals of the t_{2g} -orbital electrons on the honeycomb lattice (Fig. 1) in the presence of a light field $\mathbf{E}(t) = {}^t(E_b(t) E_a(t))$. Here $E_b(t)$ is the component antiparallel to the b axis and $E_a(t)$ is that parallel to the a axis. The $\mathbf{E}(t)$ for circularly polarized light is given by

$$\mathbf{E}_{\text{circ}}(t) = {}^t(E_0 \cos \omega t \ - E_0 \sin \omega t), \quad (2)$$

and that for linearly polarized light is given by

$$\mathbf{E}_{\text{linear-}b}(t) = {}^t(E_0 \sin \omega t \ 0) \quad (3)$$

or

$$\mathbf{E}_{\text{linear-}a}(t) = {}^t(0 \ E_0 \sin \omega t). \quad (4)$$

We do not consider the helicity of circularly polarized light because the magnetic properties shown in this paper for $\mathbf{E}(t) = \mathbf{E}_{\text{circ}}(t)$ remain unchanged even for $\mathbf{E}(t) = {}^t(E_0 \cos \omega t \ E_0 \sin \omega t)$. Then, we treat the effects of $\mathbf{E}(t)$ as Peierls phase factors:

$$H_{\text{KE}} = \sum_{i,j} \sum_{a,b} \sum_{\sigma} t_{iajb} e^{-ie(\mathbf{R}_i - \mathbf{R}_j) \cdot \mathbf{A}(t)} c_{ia\sigma}^{\dagger} c_{jb\sigma}, \quad (5)$$

TABLE I. Five cases of our model. Bond anisotropy of the nearest-neighbor hopping integrals is absent in the first and third cases and present in the other three cases. The third nearest-neighbor hopping integral is neglected in the first two cases and considered in the last three cases.

Parameter	1st	2nd	3rd	4th	5th
Bond anisotropy	Absent	Present	Absent	Present	Present
t_{3rd} (meV)	0	0	-40	-40	-60

where $A(t) = {}^t(A_b(t)A_a(t))$ for $E(t) = E_{circ}(t), E_{linear-b}(t)$, or $E_{linear-a}(t)$ is given by

$$A_{circ}(t) = {}^t\left(-\frac{E_0}{\omega} \sin \omega t \quad -\frac{E_0}{\omega} \cos \omega t\right), \quad (6)$$

$$A_{linear-b}(t) = {}^t\left(\frac{E_0}{\omega} \cos \omega t \quad 0\right), \quad (7)$$

or

$$A_{linear-a}(t) = {}^t\left(0 \quad \frac{E_0}{\omega} \cos \omega t\right), \quad (8)$$

respectively. As for t_{iajb} 's, we consider five cases (Table I). In the first case, t_{iajb} 's are parametrized by three nearest-neighbor hopping integrals [12,20]: the finite t_{iajb} 's for the Z bonds (Fig. 1) are

$$t_{idy_zjd_{yz}} = t_{id_xjd_{zx}} = t_1, \quad (9)$$

$$t_{idy_zjd_{zx}} = t_{id_xjd_{yz}} = t_2, \quad (10)$$

$$t_{id_{xy}jd_{xy}} = t_3, \quad (11)$$

and those for the X and the Y bonds are obtained by replacing (x, y, z) in Eqs. (9)–(11) by (y, z, x) and (z, x, y), respectively. This case, which is used also in our previous paper [20], corresponds to a minimal model of α -RuCl₃. In the second case, the bond anisotropy of t_1 , t_2 , and t_3 is considered: the finite t_{iajb} 's for the Z bonds are the same as Eqs. (9)–(11), whereas those for the X or the Y bonds are

$$t_{id_{zx}jd_{zx}} = t_{id_{xy}jd_{xy}} = t'_1, \quad (12)$$

$$t_{id_{zx}jd_{xy}} = t_{id_{xy}jd_{zx}} = t'_2, \quad (13)$$

$$t_{idy_zjd_{yz}} = t'_3, \quad (14)$$

or

$$t_{id_{xy}jd_{xy}} = t_{idy_zjd_{yz}} = t'_1, \quad (15)$$

$$t_{id_{xy}jd_{yz}} = t_{idy_zjd_{xy}} = t'_2, \quad (16)$$

$$t_{id_{zx}jd_{zx}} = t'_3, \quad (17)$$

respectively. This case is used to study the effects of the weak bond anisotropy [13] of α -RuCl₃ on the magnetic properties. In the third or the fourth case, we consider not only the nearest-neighbor hopping integrals considered in the first or the second case, respectively, but also a third-neighbor hopping integral t_{3rd} . The t_{3rd} for the Z₃, X₃, or Y₃ bonds (Fig. 1) is the intraorbital hopping integral of the d_{xy} , d_{yz} , or d_{zx} orbital, respectively. (We consider only this among the third neighbor hopping integrals because it is the largest [13].) The fifth case is almost the same as the fourth case except for the value of t_{3rd} (see the first paragraph of Sec. IV B). The last three cases are

used to analyze the effects of J_{3rd} , the Heisenberg interaction between third neighbors, on several magnetic states. In Sec. V, we will compare our choices of t_{iajb} 's with the result obtained in first-principles calculations [13].

The atomic SOC is given by the LS coupling of the t_{2g} -orbital electrons [8,9]. Because of its nonperturbative effect, the t_{2g} -orbital states with spin degrees of freedom are converted into the $j_{eff} = 1/2$ doublet and the $j_{eff} = 3/2$ quartet. (In this argument, we have omitted the components of the LS coupling between the t_{2g} and the e_g orbitals because the crystal field energy between them is supposed to be sufficiently large; this is the reason why the total angular momentum is not j , but j_{eff} .) For α -RuCl₃, the low-energy properties can be described by the $j_{eff} = 1/2$ doublet [25,26], which is occupied by an electron (or a hole) per site,

$$|+\rangle_i = \frac{1}{\sqrt{3}}(c_{idy_z\downarrow}^\dagger + ic_{id_x\downarrow}^\dagger + c_{id_{xy}\uparrow}^\dagger)|0\rangle, \quad (18)$$

$$|-\rangle_i = \frac{1}{\sqrt{3}}(c_{idy_z\uparrow}^\dagger - ic_{id_x\uparrow}^\dagger - c_{id_{xy}\downarrow}^\dagger)|0\rangle. \quad (19)$$

In these states, the spin and the orbital are entangled.

The Coulomb interactions are given by the multiorbital Hubbard interactions [24] of the t_{2g} -orbital electrons:

$$H_{int} = \sum_i \left\{ \sum_{a,b} c_{ia\uparrow}^\dagger c_{ia\downarrow}^\dagger [U\delta_{a,b} + J'(1 - \delta_{a,b})] c_{ib\downarrow} c_{ib\uparrow} + \sum_{\substack{a,b \\ a>b}} \sum_{\sigma,\sigma'} c_{ia\sigma}^\dagger c_{ib\sigma'}^\dagger (U' c_{ib\sigma'} c_{ia\sigma} - J_H c_{ib\sigma} c_{ia\sigma'}) \right\}, \quad (20)$$

where U , J' , U' , and J_H are the intraorbital Hubbard interaction, the pair hopping, the interorbital Hubbard interaction, and the Hund's coupling, respectively. In deriving the exchange interactions of periodically driven α -RuCl₃ (Sec. III A), we use H_{int} expressed in terms of the irreducible representations of doubly occupied states [14,20,27]:

$$H_{int} = \sum_i \sum_{\Gamma, g_\Gamma} U_\Gamma |i; \Gamma, g_\Gamma\rangle \langle i; \Gamma, g_\Gamma|, \quad (21)$$

where U_Γ 's are given by

$$U_{A_1} = U + 2J', \quad (22)$$

$$U_E = U - J', \quad (23)$$

$$U_{T_1} = U' - J_H, \quad (24)$$

$$U_{T_2} = U' + J_H, \quad (25)$$

and $|i; \Gamma, g_\Gamma\rangle$'s are given by

$$|i; A_1\rangle = \frac{1}{\sqrt{3}}(c_{id_{yz}\uparrow}^\dagger c_{id_{yz}\downarrow}^\dagger + c_{id_{zx}\uparrow}^\dagger c_{id_{zx}\downarrow}^\dagger + c_{id_{xy}\uparrow}^\dagger c_{id_{xy}\downarrow}^\dagger)|0\rangle, \quad (26)$$

$$|i; E, u\rangle = \frac{1}{\sqrt{6}}(c_{id_{yz}\uparrow}^\dagger c_{id_{yz}\downarrow}^\dagger + c_{id_{zx}\uparrow}^\dagger c_{id_{zx}\downarrow}^\dagger - 2c_{id_{xy}\uparrow}^\dagger c_{id_{xy}\downarrow}^\dagger)|0\rangle, \quad (27)$$

$$|i; E, v\rangle = \frac{1}{\sqrt{2}}(c_{id_{yz}\uparrow}^\dagger c_{id_{yz}\downarrow}^\dagger - c_{id_{zx}\uparrow}^\dagger c_{id_{zx}\downarrow}^\dagger)|0\rangle, \quad (28)$$

$$|i; T_1, \alpha_+\rangle = c_{id_{yz}\uparrow}^\dagger c_{id_{zx}\uparrow}^\dagger|0\rangle, \quad (29)$$

$$|i; T_1, \alpha_-\rangle = c_{id_{yz}\downarrow}^\dagger c_{id_{zx}\downarrow}^\dagger|0\rangle, \quad (30)$$

$$|i; T_1, \alpha\rangle = \frac{1}{\sqrt{2}}(c_{id_{yz}\uparrow}^\dagger c_{id_{zx}\downarrow}^\dagger + c_{id_{yz}\downarrow}^\dagger c_{id_{zx}\uparrow}^\dagger)|0\rangle, \quad (31)$$

$$|i; T_1, \beta_+\rangle = c_{id_{zx}\uparrow}^\dagger c_{id_{xy}\uparrow}^\dagger|0\rangle, \quad (32)$$

$$|i; T_1, \beta_-\rangle = c_{id_{zx}\downarrow}^\dagger c_{id_{xy}\downarrow}^\dagger|0\rangle, \quad (33)$$

$$|i; T_1, \beta\rangle = \frac{1}{\sqrt{2}}(c_{id_{zx}\uparrow}^\dagger c_{id_{xy}\downarrow}^\dagger + c_{id_{zx}\downarrow}^\dagger c_{id_{xy}\uparrow}^\dagger)|0\rangle, \quad (34)$$

$$|i; T_1, \gamma_+\rangle = c_{id_{xy}\uparrow}^\dagger c_{id_{yz}\uparrow}^\dagger|0\rangle, \quad (35)$$

$$|i; T_1, \gamma_-\rangle = c_{id_{xy}\downarrow}^\dagger c_{id_{yz}\downarrow}^\dagger|0\rangle, \quad (36)$$

$$|i; T_1, \gamma\rangle = \frac{1}{\sqrt{2}}(c_{id_{xy}\uparrow}^\dagger c_{id_{yz}\downarrow}^\dagger + c_{id_{xy}\downarrow}^\dagger c_{id_{yz}\uparrow}^\dagger)|0\rangle, \quad (37)$$

$$|i; T_2, \alpha\rangle = \frac{1}{\sqrt{2}}(c_{id_{yz}\uparrow}^\dagger c_{id_{zx}\downarrow}^\dagger - c_{id_{yz}\downarrow}^\dagger c_{id_{zx}\uparrow}^\dagger)|0\rangle, \quad (38)$$

$$|i; T_2, \beta\rangle = \frac{1}{\sqrt{2}}(c_{id_{zx}\uparrow}^\dagger c_{id_{xy}\downarrow}^\dagger - c_{id_{zx}\downarrow}^\dagger c_{id_{xy}\uparrow}^\dagger)|0\rangle, \quad (39)$$

$$|i; T_2, \gamma\rangle = \frac{1}{\sqrt{2}}(c_{id_{xy}\uparrow}^\dagger c_{id_{yz}\downarrow}^\dagger - c_{id_{xy}\downarrow}^\dagger c_{id_{yz}\uparrow}^\dagger)|0\rangle. \quad (40)$$

III. EXCHANGE INTERACTIONS

In this section, we study the exchange interactions of periodically driven α -RuCl₃. In Sec. III A, we derive an effective Hamiltonian expressed in terms of the exchange interactions in the strong-interaction limit for a high-frequency case of the driving field. This derivation is performed in the first case of our model, and the changes in the last four cases are also remarked on. In Sec. III B, we present the dependences of the exchange interactions on the dimensionless parameter $|u_{ij}|$ for some nonresonant values of ω . The reason why we use nonresonant ω 's is that our theory is valid only for such ω 's [see the derivation of Eq. (57)]. We also discuss the effects of circularly or linearly polarized light and the similarities and differences between them.

A. Theory

We derive the exchange interactions of our periodically driven Mott insulator with strong SOC. Since the derivation for circularly polarized light has been described in our previous paper [20], we explain the main points and some changes for linearly polarized light. Here we derive the expression in

the first case of our model; the expressions in the other four cases can be obtained from symmetry arguments (see the fifth paragraph of this section). The derivation consists of three steps.

First, we derive an effective Hamiltonian for the periodically driven Mott insulator with strong SOC. To do this, we consider the strong-interaction limit in which t_{iajb} 's in Eq. (5) are much smaller than U_Γ 's in Eq. (21). In this limit, the solution to Schrödinger's equation can be approximately expressed as $|\Psi\rangle_t \approx |\Psi_0\rangle_t + |\Psi_1\rangle_t$ with $|\Psi_0\rangle_t$ and $|\Psi_1\rangle_t$, the states without and with, respectively, a doubly occupied site. Thus, the solution can be obtained by solving a set of simultaneous equations,

$$i\partial_t|\Psi_0\rangle_t = \mathcal{P}_0 H_{\text{KE}}|\Psi_1\rangle_t + H_{\text{SOC}}|\Psi_0\rangle_t, \quad (41)$$

$$i\partial_t|\Psi_1\rangle_t = H_{\text{KE}}|\Psi_0\rangle_t + (\mathcal{P}_1 H_{\text{KE}} \mathcal{P}_1 + \tilde{H}_{\text{int}})|\Psi_1\rangle_t, \quad (42)$$

where \mathcal{P}_0 and \mathcal{P}_1 denote the projections onto the subspaces without and with, respectively, a doubly occupied site, and \tilde{H}_{int} is defined as

$$\tilde{H}_{\text{int}} = H_{\text{int}} + H_{\text{SOC}}. \quad (43)$$

Then, we suppose that ω is much larger than t_{iajb} 's. In this situation, $\mathcal{P}_1 H_{\text{KE}} \mathcal{P}_1$ in Eq. (42) could be replaced by its time-averaged one \bar{H}_{KE} . As derived in Appendix A, \bar{H}_{KE} is given by

$$\bar{H}_{\text{KE}} = \mathcal{P}_1 \sum_{i,j} \sum_{a,b} \sum_{\sigma} t_{iajb} \mathcal{J}_0[\tilde{u}_{ij}^{(p)}] c_{ia\sigma}^\dagger c_{jb\sigma} \mathcal{P}_1, \quad (44)$$

where $\mathcal{J}_n(x)$ is the n th Bessel function of the first kind, $\tilde{u}_{ij}^{(p)}$'s for $\mathbf{A}(t) = \mathbf{A}_{\text{circ}}(t)$, $\mathbf{A}_{\text{linear-}b}(t)$, and $\mathbf{A}_{\text{linear-}a}(t)$ are given by

$$\tilde{u}_{ij}^{(c)} = u_{ij} = \frac{eE_0}{\omega} \text{sgn}(i-j), \quad (45)$$

$$\tilde{u}_{ij}^{(\text{lb})} = \begin{cases} \frac{1}{2}u_{ij} & (X \text{ or } Y \text{ bonds}), \\ u_{ij} & (Z \text{ bonds}), \end{cases} \quad (46)$$

and

$$\tilde{u}_{ij}^{(\text{la})} = \begin{cases} \frac{\sqrt{3}}{2}u_{ij} & (X \text{ or } Y \text{ bonds}), \\ 0 & (Z \text{ bonds}), \end{cases} \quad (47)$$

respectively, and $\text{sgn}(i-j)$ is 1 for $i \in A$ or -1 for $i \in B$. (Note that $i \in A$ or $i \in B$ means that i is on the A sublattice or on the B sublattice, respectively.) By using the replacement $\mathcal{P}_1 H_{\text{KE}} \mathcal{P}_1 \rightarrow \bar{H}_{\text{KE}}$, we can write Eq. (42) as

$$(i\partial_t - \bar{H}_{\text{KE}} - \tilde{H}_{\text{int}})|\Psi_1\rangle_t = H_{\text{KE}}|\Psi_0\rangle_t. \quad (48)$$

This is equivalent to the following equation:

$$i\partial_t [e^{i(\bar{H}_{\text{KE}} + \tilde{H}_{\text{int}})t} |\Psi_1\rangle_t] = e^{i(\bar{H}_{\text{KE}} + \tilde{H}_{\text{int}})t} H_{\text{KE}}|\Psi_0\rangle_t. \quad (49)$$

As derived in Appendix B, the solution to Eq. (49) can be expressed as follows:

$$|\Psi_1\rangle_t = \sum_{i,j,a,b,\sigma} \sum_{n=-\infty}^{\infty} \frac{t_{iajb} \tilde{\mathcal{J}}_{-nv_{ij}}^{(p)}(u_{ij}) e^{-in\omega t}}{n\omega - \bar{H}_{\text{KE}} - \tilde{H}_{\text{int}}} c_{ia\sigma}^\dagger c_{jb\sigma} |\Psi_0\rangle_t, \quad (50)$$

where $\tilde{\mathcal{J}}_{-nv_{ij}}^{(p)}(u_{ij})$'s for $A(t) = A_{\text{circ}}(t)$, $A_{\text{linear-}b}(t)$, and $A_{\text{linear-}a}(t)$ are given by

$$\tilde{\mathcal{J}}_{-nv_{ij}}^{(c)}(u_{ij}) = \begin{cases} \mathcal{J}_{-n}(u_{ij})e^{-in\frac{\pi}{3}} & (v_{ij} = X), \\ \mathcal{J}_{-n}(u_{ij})e^{-in\frac{\pi}{3}} & (v_{ij} = Y), \\ \mathcal{J}_{-n}(u_{ij})e^{-in\pi} & (v_{ij} = Z), \end{cases} \quad (51)$$

$$\tilde{\mathcal{J}}_{-nv_{ij}}^{(lb)}(u_{ij}) = \begin{cases} \mathcal{J}_{-n}\left(\frac{u_{ij}}{2}\right)e^{+in\frac{\pi}{2}} & (v_{ij} = X), \\ \mathcal{J}_{-n}\left(\frac{u_{ij}}{2}\right)e^{+in\frac{\pi}{2}} & (v_{ij} = Y), \\ \mathcal{J}_{-n}(u_{ij})e^{-in\frac{\pi}{2}} & (v_{ij} = Z), \end{cases} \quad (52)$$

and

$$\tilde{\mathcal{J}}_{-nv_{ij}}^{(la)}(u_{ij}) = \begin{cases} \mathcal{J}_{-n}\left(\frac{\sqrt{3}}{2}u_{ij}\right)e^{-in\frac{\pi}{2}} & (v_{ij} = X), \\ \mathcal{J}_{-n}\left(\frac{\sqrt{3}}{2}u_{ij}\right)e^{+in\frac{\pi}{2}} & (v_{ij} = Y), \\ \delta_{n,0} & (v_{ij} = Z), \end{cases} \quad (53)$$

respectively. By substituting Eq. (50) into Eq. (41) and omitting the constant term $H_{\text{SOC}}|\Psi_0\rangle_t$, we obtain

$$i\partial_t|\Psi_0\rangle_t = H_{\text{eff}}(t)|\Psi_0\rangle_t, \quad (54)$$

where

$$H_{\text{eff}}(t) = \sum_{i,j,i',j'} \sum_{n,m=-\infty}^{\infty} \mathcal{P}_0 T_{i'j'} \tilde{\mathcal{J}}_{mv_{i'j'}}^{(p)}(u_{i'j'}) \times \frac{e^{i(m-n)\omega t}}{n\omega - \bar{H}_{\text{KE}} - \bar{H}_{\text{int}}} \tilde{\mathcal{J}}_{-nv_{ij}}^{(p)}(u_{ij}) T_{ij} \mathcal{P}_0, \quad (55)$$

and

$$T_{ij} = \sum_{a,b} \sum_{\sigma} t_{ia,jb} c_{ia\sigma}^\dagger c_{jb\sigma}. \quad (56)$$

Furthermore, since in the denominator of Eq. (55) H_{int} gives the largest contribution of \bar{H}_{KE} and $\bar{H}_{\text{int}} (= H_{\text{int}} + H_{\text{SOC}})$, we replace $n\omega - \bar{H}_{\text{KE}} - \bar{H}_{\text{int}}$ in Eq. (55) by $n\omega - H_{\text{int}}$; this replacement may be sufficient for nonresonant ω 's (i.e., the ω 's at which the denominator does not diverge). As a result, we have

$$H_{\text{eff}}(t) = \sum_{i,j} \sum_{n,m=-\infty}^{\infty} \mathcal{P}_0 T_{ji} \tilde{\mathcal{J}}_{mv_{ji}}^{(p)}(u_{ji}) \times \frac{e^{i(m-n)\omega t}}{n\omega - H_{\text{int}}} \tilde{\mathcal{J}}_{-nv_{ij}}^{(p)}(u_{ij}) T_{ij} \mathcal{P}_0. \quad (57)$$

Second, we derive the leading term of $H_{\text{eff}}(t)$. By expressing $H_{\text{eff}}(t)$ as the Fourier series $H_{\text{eff}}(t) = \sum_l e^{il\omega t} H_l$ and using a high-frequency expansion of the Floquet theory [3], we can write $H_{\text{eff}}(t)$ in the form

$$H_{\text{eff}}(t) = H_0 + O\left(\frac{J_{\text{ex}}^2}{\omega}\right), \quad (58)$$

where J_{ex} is of the order of the exchange interactions. If ω is high enough to satisfy $\omega \gg |J_{\text{ex}}|$, the leading term of $H_{\text{eff}}(t)$ comes from the Floquet Hamiltonian $\bar{H}_{\text{eff}} (= H_0)$:

$$\begin{aligned} \bar{H}_{\text{eff}} &= \frac{\omega}{2\pi} \int_0^{2\pi/\omega} dt H_{\text{eff}}(t) \\ &= \sum_{i,j} \sum_{n=-\infty}^{\infty} \mathcal{P}_0 T_{ji} \frac{\mathcal{J}_n[\tilde{u}_{ij}^{(p)}]^2}{n\omega - H_{\text{int}}} T_{ij} \mathcal{P}_0. \end{aligned} \quad (59)$$

Furthermore, by using Eq. (21) and expressing the projection operators \mathcal{P}_0 's in terms of the possible states, we can rewrite Eq. (59) as follows:

$$\begin{aligned} \bar{H}_{\text{eff}} &= \sum_{i,j} \sum_{n=-\infty}^{\infty} \sum_{\Gamma, g_\Gamma} \mathcal{P}_0 T_{ji} |i; \Gamma, g_\Gamma\rangle \frac{\mathcal{J}_n[\tilde{u}_{ij}^{(p)}]^2}{n\omega - U_\Gamma} \\ &\quad \times \langle i; \Gamma, g_\Gamma | T_{ij} \mathcal{P}_0 \\ &= \sum_{i,j} \sum_{n=-\infty}^{\infty} \sum_{\Gamma, g_\Gamma} \sum_{i,f} \langle f | T_{ji} | i; \Gamma, g_\Gamma\rangle \frac{\mathcal{J}_n[\tilde{u}_{ij}^{(p)}]^2}{n\omega - U_\Gamma} \\ &\quad \times \langle i; \Gamma, g_\Gamma | T_{ij} | i \rangle |f\rangle \langle i|, \end{aligned} \quad (60)$$

where $|i\rangle$ and $|f\rangle$ are restricted to the $j_{\text{eff}} = 1/2$ subspace. Equation (60) shows that a light field affects the effective Hamiltonian through the factor $\mathcal{J}_n[\tilde{u}_{ij}^{(p)}]^2/(n\omega - U_\Gamma)$ (i.e., the changes due to the Bessel functions and the energy shifts of intermediate states). Note that if we replace $\sum_{n=-\infty}^{\infty} \mathcal{J}_n[\tilde{u}_{ij}^{(p)}]^2/(n\omega - U_\Gamma)$ in Eq. (60) by $1/(-U_\Gamma)$, the resultant equation gives the effective Hamiltonian in the absence of $E(t)$.

Third, we express Eq. (60) in terms of exchange interactions. To do this, we calculate the possible terms for the Z bonds on the honeycomb lattice; the other terms can be obtained from symmetry arguments. T_{ij} for the Z bonds, T_{ij}^Z , is given by

$$\begin{aligned} T_{ij}^Z &= t_1 \sum_{\sigma} (c_{id_{y\sigma}}^\dagger c_{jd_{y\sigma}} + c_{id_{x\sigma}}^\dagger c_{jd_{x\sigma}}) \\ &\quad + t_2 \sum_{\sigma} (c_{id_{y\sigma}}^\dagger c_{jd_{x\sigma}} + c_{id_{x\sigma}}^\dagger c_{jd_{y\sigma}}) \\ &\quad + t_3 \sum_{\sigma} c_{id_{xy\sigma}}^\dagger c_{jd_{xy\sigma}}. \end{aligned} \quad (61)$$

Then, since Eq. (60) is the sum of two-site terms, we express $|i\rangle$ and $|f\rangle$ as the products of the $j_{\text{eff}} = 1/2$ states at two sites:

$$\{|i\rangle, |f\rangle\} = \{|+, +\rangle, |+, -\rangle, |-, +\rangle, |-, -\rangle\}, \quad (62)$$

where $|+, +\rangle = |+\rangle_1 |+\rangle_2$, $|+, -\rangle = |+\rangle_1 |-\rangle_2$, $|-, +\rangle = |-\rangle_1 |+\rangle_2$, and $|-, -\rangle = |-\rangle_1 |-\rangle_2$; $|+\rangle_i$ and $|-\rangle_i$ have been defined in Eqs. (18) and (19). Since $|i; \Gamma, g_\Gamma\rangle$'s and U_Γ 's are given by Eqs. (26)–(40) and Eqs. (22)–(25), we can write the finite terms of Eq. (60) for the Z bonds in the form

$$\sum_{(i,j)_Z} [J_Z \mathbf{S}_i \cdot \mathbf{S}_j + K_Z S_i^z S_j^z + \Gamma_Z (S_i^x S_j^y + S_i^y S_j^x)], \quad (63)$$

where the summation $\sum_{(i,j)_Z}$ is over all the Z bonds,

$$\begin{aligned} J_Z &= \sum_{n=-\infty}^{\infty} \frac{4\mathcal{J}_n(u_{ij}^Z)^2}{27} \left[\frac{(2t_1 + t_3)^2}{U + 2J' - n\omega} + \frac{6t_1(t_1 + 2t_3)}{U' - J_H - n\omega} \right. \\ &\quad \left. + \frac{2[(t_1 - t_3)^2 - 3t_2^2]}{U - J' - n\omega} + \frac{6t_2^2}{U' + J_H - n\omega} \right], \end{aligned} \quad (64)$$

$$\begin{aligned} K_Z &= \sum_{n=-\infty}^{\infty} \frac{4\mathcal{J}_n(u_{ij}^Z)^2}{9} \left[\frac{4t_2^2}{U - J' - n\omega} - \frac{(t_1 - t_3)^2 + t_2^2}{U' + J_H - n\omega} \right. \\ &\quad \left. - \frac{3t_2^2 - (t_1 - t_3)^2}{U' - J_H - n\omega} \right], \end{aligned} \quad (65)$$

$$\Gamma_Z = \sum_{n=-\infty}^{\infty} \frac{8\mathcal{J}_n(u_{ij}^Z)^2}{9} \left[\frac{t_2(t_1 - t_3)}{U' - J_H - n\omega} - \frac{t_2(t_1 - t_3)}{U' + J_H - n\omega} \right], \quad (66)$$

and

$$u_{ij}^Z = \begin{cases} u_{ij} & \text{for } \mathbf{A}(t) = \mathbf{A}_{\text{circ}}(t), \\ u_{ij} & \text{for } \mathbf{A}(t) = \mathbf{A}_{\text{linear-}b}(t), \\ 0 & \text{for } \mathbf{A}(t) = \mathbf{A}_{\text{linear-}a}(t). \end{cases} \quad (67)$$

The derivation of Eq. (63) is described in Appendix C. Equations (64)–(67) show that for $\mathbf{A}(t) = \mathbf{A}_{\text{circ}}(t)$ and $\mathbf{A}_{\text{linear-}b}(t)$ J_Z , K_Z , and Γ_Z can be changed by varying ω , E_0 , or both, whereas for $\mathbf{A}(t) = \mathbf{A}_{\text{linear-}a}(t)$ those remain unchanged due to $\mathcal{J}_n(0) = \delta_{n,0}$. This means that the exchange interactions for the Z bonds are not affected if the light is polarized along the a axis. Then, replacing (x, y, z, Z) in Eq. (63) by (y, z, x, X) or (z, x, y, Y) , we obtain the possible terms for the X or the Y bonds, respectively. As a result, \bar{H}_{eff} 's for the X and the Y bonds are given by

$$\sum_{(i,j)_X} [J_X \mathbf{S}_i \cdot \mathbf{S}_j + K_X S_i^x S_j^x + \Gamma_X (S_i^y S_j^z + S_i^z S_j^y)] \quad (68)$$

and

$$\sum_{(i,j)_Y} [J_Y \mathbf{S}_i \cdot \mathbf{S}_j + K_Y S_i^y S_j^y + \Gamma_Y (S_i^z S_j^x + S_i^x S_j^z)], \quad (69)$$

respectively. Here the summations $\sum_{(i,j)_X}$ and $\sum_{(i,j)_Y}$ are over all the X and the Y bonds, respectively; J_X , J_Y , K_X , K_Y , Γ_X , and Γ_Y are given by

$$\begin{aligned} J_X &= J_Y \\ &= \sum_{n=-\infty}^{\infty} \frac{4\mathcal{J}_n(u_{ij}^X)^2}{27} \left[\frac{(2t_1 + t_3)^2}{U + 2J' - n\omega} + \frac{6t_1(t_1 + 2t_3)}{U' - J_H - n\omega} \right. \\ &\quad \left. + \frac{2[(t_1 - t_3)^2 - 3t_2^2]}{U - J' - n\omega} + \frac{6t_2^2}{U' + J_H - n\omega} \right], \end{aligned} \quad (70)$$

$$\begin{aligned} K_X &= K_Y \\ &= \sum_{n=-\infty}^{\infty} \frac{4\mathcal{J}_n(u_{ij}^X)^2}{9} \left[\frac{4t_2^2}{U - J' - n\omega} - \frac{(t_1 - t_3)^2 + t_2^2}{U' + J_H - n\omega} \right. \\ &\quad \left. - \frac{3t_2^2 - (t_1 - t_3)^2}{U' - J_H - n\omega} \right], \end{aligned} \quad (71)$$

$$\begin{aligned} \Gamma_X &= \Gamma_Y \\ &= \sum_{n=-\infty}^{\infty} \frac{8\mathcal{J}_n(u_{ij}^X)^2}{9} \left[\frac{t_2(t_1 - t_3)}{U' - J_H - n\omega} - \frac{t_2(t_1 - t_3)}{U' + J_H - n\omega} \right], \end{aligned} \quad (72)$$

where

$$u_{ij}^X = \begin{cases} u_{ij} & \text{for } \mathbf{A}(t) = \mathbf{A}_{\text{circ}}(t), \\ \frac{1}{2}u_{ij} & \text{for } \mathbf{A}(t) = \mathbf{A}_{\text{linear-}b}(t), \\ \frac{\sqrt{3}}{2}u_{ij} & \text{for } \mathbf{A}(t) = \mathbf{A}_{\text{linear-}a}(t). \end{cases} \quad (73)$$

Comparing Eqs. (70)–(73) with Eqs. (64)–(67), we see linearly polarized light can induce the bond anisotropy of the

exchange interactions, i.e., the differences between the exchange interactions for the Z bonds and those for the X or Y bonds, even without the bond anisotropy of the hopping integrals. Such light-induced bond anisotropy does not appear for circularly polarized light. The origin of this light-induced bond anisotropy is the difference in the argument of the Bessel function [Eqs. (67) and (73)]. In Sec. III B, we will analyze the light-induced bond anisotropy quantitatively. Then, by combining Eqs. (68) and (69) with Eq. (63), we can express \bar{H}_{eff} as follows:

$$\bar{H}_{\text{eff}} = \sum_{(i,j)} [J_\delta \mathbf{S}_i \cdot \mathbf{S}_j + K_\delta S_i^\gamma S_j^\gamma + \Gamma_\delta (S_i^\alpha S_j^\beta + S_i^\beta S_j^\alpha)], \quad (74)$$

where

$$(\alpha, \beta, \gamma, \delta) = \begin{cases} (y, z, x, X) & (X \text{ bonds}), \\ (z, x, y, Y) & (Y \text{ bonds}), \\ (x, y, z, Z) & (Z \text{ bonds}). \end{cases} \quad (75)$$

Before showing the results obtained in numerical calculations, we comment on the exchange interactions in the other four cases of our model. In the second case, in which the bond anisotropy of t_1 , t_2 , and t_3 is considered [Eqs. (12)–(17)], the exchange interactions for the X and Y bonds are given by

$$\begin{aligned} J_X &= J_Y \\ &= \sum_{n=-\infty}^{\infty} \frac{4\mathcal{J}_n(u_{ij}^X)^2}{27} \left[\frac{(2t'_1 + t'_3)^2}{U + 2J' - n\omega} + \frac{6t'_1(t'_1 + 2t'_3)}{U' - J_H - n\omega} \right. \\ &\quad \left. + \frac{2[(t'_1 - t'_3)^2 - 3(t'_2)^2]}{U - J' - n\omega} + \frac{6(t'_2)^2}{U' + J_H - n\omega} \right], \end{aligned} \quad (76)$$

$$\begin{aligned} K_X &= K_Y \\ &= \sum_{n=-\infty}^{\infty} \frac{4\mathcal{J}_n(u_{ij}^X)^2}{9} \left[\frac{4(t'_2)^2}{U - J' - n\omega} - \frac{(t'_1 - t'_3)^2 + (t'_2)^2}{U' + J_H - n\omega} \right. \\ &\quad \left. - \frac{3(t'_2)^2 - (t'_1 - t'_3)^2}{U' - J_H - n\omega} \right], \end{aligned} \quad (77)$$

$$\begin{aligned} \Gamma_X &= \Gamma_Y \\ &= \sum_{n=-\infty}^{\infty} \frac{8\mathcal{J}_n(u_{ij}^X)^2}{9} \left[\frac{t'_2(t'_1 - t'_3)}{U' - J_H - n\omega} - \frac{t'_2(t'_1 - t'_3)}{U' + J_H - n\omega} \right], \end{aligned} \quad (78)$$

rather than by Eqs. (70)–(72); those for the Z bonds are given by Eqs. (64)–(66). Thus, by comparing the results in this case and the first case, we can understand how the light-induced bond anisotropy of the exchange interactions is affected by the bond anisotropy of the nearest-neighbor hopping integrals. Those results are shown in Sec. III B. In Sec. IV B, we will analyze the energies of several magnetic states not only in those cases, but also in the additional three cases. In the latter three cases, we consider the third-neighbor hopping integral $t_{3\text{rd}}$, as well as the nearest-neighbor hopping integrals; it leads to the third-neighbor Heisenberg interaction

$$\sum_{\langle\langle\langle i,j \rangle\rangle\rangle} J_\delta^{\text{3rd}} \mathbf{S}_i \cdot \mathbf{S}_j, \quad (79)$$

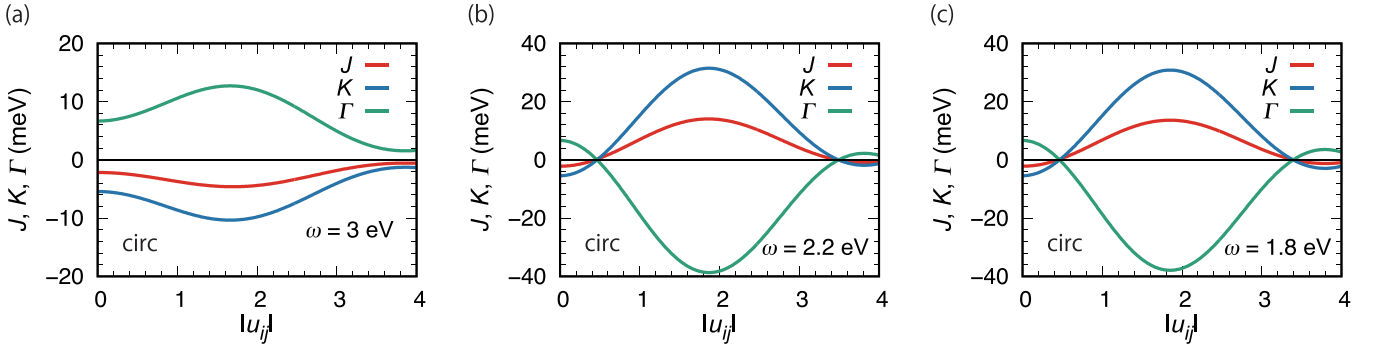


FIG. 2. The $|u_{ij}| (=|\frac{eE_0}{\omega}|)$ dependences of J , K , and Γ with $\mathbf{E}_{\text{circ}}(t)$ at (a) $\omega = 3$, (b) 2.2, and (c) 1.8 eV in the first case of our model. In this case, there is no bond anisotropy of the exchange interactions: $J_Z = J_X = J_Y = J$, $K_Z = K_X = K_Y = K$, and $\Gamma_Z = \Gamma_X = \Gamma_Y = \Gamma$.

where the summation $\sum_{\langle\langle(i,j)\rangle\rangle}$ is over all the Z_3 , X_3 , and Y_3 bonds (Fig. 1), δ is Z , X , or Y for the Z_3 , X_3 , or Y_3 bonds, respectively, and J_δ^{3rd} is given (in the second-order perturbation theory) by

$$J_\delta^{\text{3rd}} = \sum_{n=-\infty}^{\infty} \frac{4\mathcal{J}_n(2u_{ij}^\delta)^2}{27} \left(\frac{t_{3\text{rd}}^2}{U + 2J' - n\omega} + \frac{2t_{3\text{rd}}^2}{U - J' - n\omega} \right). \quad (80)$$

[For example, J_Z^{3rd} is obtained by replacing u_{ij}^Z , t_3 , t_1 , and t_2 in Eq. (64) by $2u_{ij}^Z$, $t_{3\text{rd}}$, 0, and 0, respectively.] In the third case of our model, the effective Hamiltonian consists of the sum of Eqs. (74) and (79) with Eqs. (64)–(67), (70)–(73), and (80). In the fourth or the fifth case, the effective Hamiltonian is the same as that in the third case except that the exchange interactions for the X and the Y bonds are given by Eqs. (76)–(78). Analyses of several magnetic states in those three cases may be useful to clarify the role of J_δ^{3rd} , which is shown to be important without $\mathbf{E}(t)$ [13], in determining the magnetic states of periodically driven α -RuCl₃.

In our analyses, we do not consider the third-neighbor Kitaev interaction K_δ^{3rd} , although it is also induced by $t_{3\text{rd}}$. This is because the value of K_δ^{3rd} is overestimated if the third-neighbor hopping integrals other than $t_{3\text{rd}}$ are omitted (the value of K_δ^{3rd} is very small in a more realistic situation [13]). In contrast to K_δ^{3rd} , the value of J_δ^{3rd} is underestimated. For more details about the values of J_δ^{3rd} and K_δ^{3rd} , see Appendix D.

B. Results

We numerically evaluate the exchange interactions for some nonresonant ω 's in the first two cases of our model. To do this, we replace $\sum_{n=-\infty}^{\infty}$'s in the exchange interactions by $\sum_{n=-n_{\text{max}}}^{n_{\text{max}}}$'s and set $n_{\text{max}} = 500$; in the first case the exchange interactions are given by Eqs. (64)–(66) and Eqs. (70)–(72), whereas in the second case those are given by Eqs. (64)–(66) and Eqs. (76)–(78). Furthermore, we set $J' = J_{\text{H}}$, $U' = U - 2J_{\text{H}}$, $U = 3$ eV, and $J_{\text{H}} = 0.5$ eV. We choose the values of the nearest-neighbor hopping integrals as follows: in the first case $t_1 = 47$ meV, $t_2 = 160$ meV, and $t_3 = -129$ meV; in the second case $t_1 = 51$ meV, $t_2 = 158$ meV, $t_3 = -154$ meV, $t'_1 = 45$ meV, $t'_2 = 162$ meV, and $t'_3 = -103$ meV. The values in the first case correspond to the averages [20] of the values obtained in the first-principles calculations (e.g., t_1 is the aver-

age of t_1 , t'_{1a} , and t'_{1b} of Ref. [13]); and the values in the second case are consistent with those obtained in the first-principles calculations [13] except that t'_1 is the average of t'_{1a} and t'_{1b} (i.e., the tiny difference between them is neglected in our analyses).

First, we present the $|u_{ij}|$ dependences of the exchange interactions with circularly polarized light. Those in the first case at $\omega = 3$, 2.2, and 1.8 eV are shown in Figs. 2(a)–2(c). We see that only the magnitudes of the exchange interactions are changed at $\omega = 3$ eV, whereas their magnitudes and signs can be changed at $\omega = 2.2$ and 1.8 eV. This property remains unchanged in the second case [Figs. 3(a)–3(f)]. The main difference between the results in these two cases is that there is no bond anisotropy of the exchange interactions in the first case (i.e., $J_Z = J_X = J_Y = J$, $K_Z = K_X = K_Y = K$, and $\Gamma_Z = \Gamma_X = \Gamma_Y = \Gamma$), whereas it is induced by the bond anisotropy of the nearest-neighbor hopping integrals in the second case. Note that at $|u_{ij}| = 0$ in the latter case we have $J_X/J_Z \sim 0.63$, $K_X/K_Z \sim 1.7$, and $\Gamma_X/\Gamma_Z \sim 0.74$, which are consistent with the values obtained in the first-principles calculations [13] (i.e., $J_X/J_Z \sim 0.64$, $K_X/K_Z \sim 1.5$, and $\Gamma_X/\Gamma_Z \sim 0.74$).

Before showing the results with linearly polarized light, we explain the mechanism of the magnitude or sign changes in the exchange interactions. Here we focus on the $|u_{ij}|$ dependences of J in the first case at $\omega = 3$ and 2.2 eV. This is enough in understanding the magnitude or sign changes shown above because of the following three facts: J , K , and Γ have the similar $|u_{ij}|$ dependences; the results at $\omega = 1.8$ eV are essentially the same as those at $\omega = 2.2$ eV; and the $|u_{ij}|$ dependences of the exchange interactions in the second case are similar to those in the first case. As we explain below, the magnitude changes and the difference in the sign changes can be understood by considering the leading terms of Eq. (64), the $n = 0$ and the $n = 1$ terms. At $\omega = 3$ eV in the first case, we can express the leading terms of $J (=J_Z)$ as follows:

$$J \approx (J_1 + J_2 + J_3)\mathcal{J}_0(u_{ij})^2 + (c'_1 J_1 - c'_2 J_2)\mathcal{J}_1(u_{ij})^2 \approx (J_2 + J_3)\mathcal{J}_0(u_{ij})^2 - c'_2 J_2 \mathcal{J}_1(u_{ij})^2, \quad (81)$$

where $J_1 = \frac{4(2t_1+t_3)^2}{27(U+2J_{\text{H}})}$, $J_2 = \frac{8(t_1-t_3)^2}{27(U-J_{\text{H}})}$, $J_3 = \frac{8t_1(t_1+2t_3)}{9(U-3J_{\text{H}})}$, $c'_1 = \frac{U+2J_{\text{H}}}{\delta\omega'_1}$, $c'_2 = \frac{U-J_{\text{H}}}{\delta\omega'_2}$, and $\omega = U - J_{\text{H}} + \delta\omega'_2 = U + 2J_{\text{H}} - \delta\omega'_1$ (i.e., $\delta\omega'_2 = 0.5$ eV and $\delta\omega'_1 = 1$ eV at $\omega = 3$ eV). In deriving the second line of Eq. (81), we have used $J_1 \ll J_2, |J_3|$, which is satisfied in α -RuCl₃. Because of this property, the $|u_{ij}|$ dependence of J is similar to those of K and Γ , as described

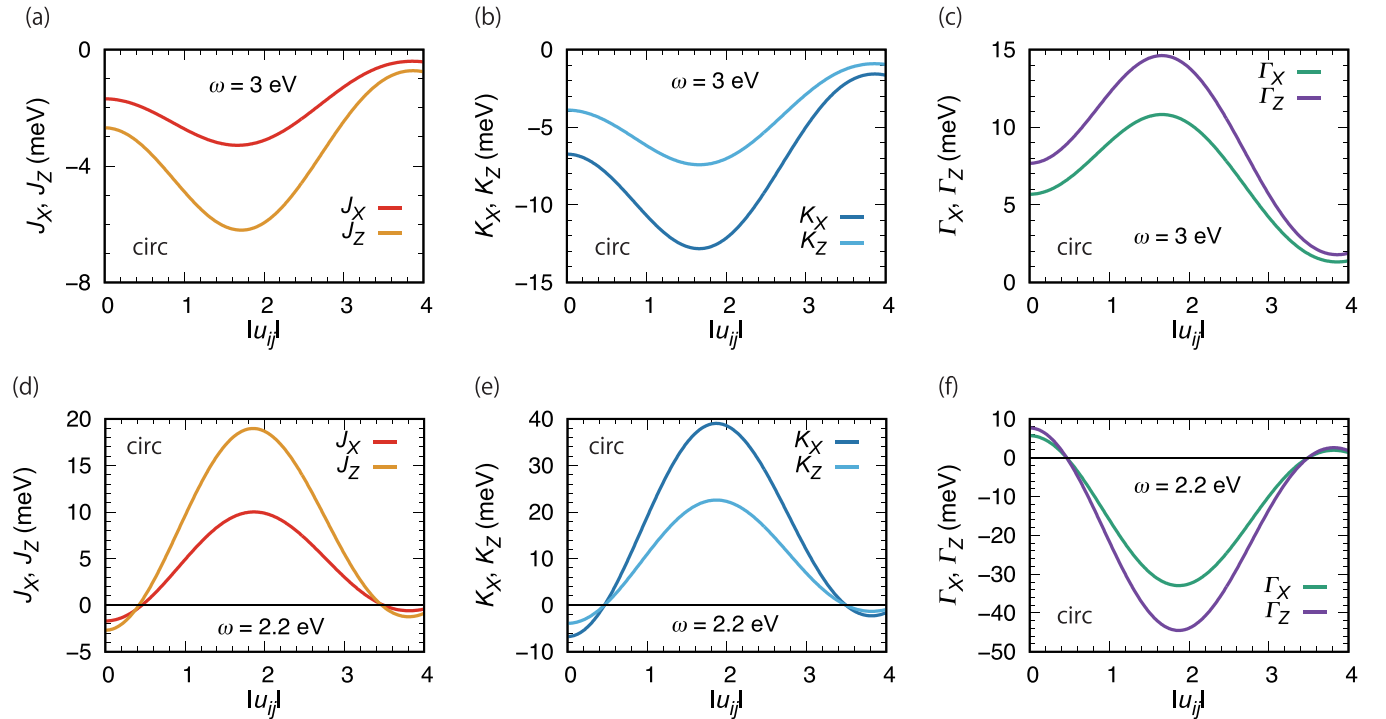


FIG. 3. The $|u_{ij}| (= |\frac{eE_0}{\omega}|)$ dependences of $J_X (=J_Y)$, J_Z , $K_X (=K_Y)$, K_Z , $\Gamma_X (= \Gamma_Y)$, and Γ_Z with $\mathbf{E}_{\text{circ}}(t)$ in the second case of our model. The value of ω is 3 eV in (a)–(c) and 2.2 eV in (d)–(f). In contrast to the first case with $\mathbf{E}_{\text{circ}}(t)$ (Fig. 2), the exchange interactions become bond-anisotropic due to the bond anisotropy of the nearest-neighbor hopping integrals.

in Ref. [20]. Since $J_2 > 0$, $J_3 < 0$, and $J_2 + J_3 < 0$ are also satisfied, Eq. (81) shows that J is always negative, i.e., its sign remains unchanged, although its magnitude is changed due to the Bessel functions. Then, at $\omega = 2.2$ eV in the first case, the leading terms of Eq. (64) are given by

$$J \approx (J_2 + J_3)\mathcal{J}_0(u_{ij})^2 + (c_2J_2 - c_3J_3)\mathcal{J}_1(u_{ij})^2, \quad (82)$$

where $c_2 = \frac{U-J_H}{\delta\omega_2}$, $c_3 = \frac{U-3J_H}{\delta\omega_3}$, and $\omega = U - 3J_H + \delta\omega_3 = U - J_H - \delta\omega_2$ (i.e., $\delta\omega_3 = 0.7$ eV and $\delta\omega_2 = 0.3$ eV at $\omega = 2.2$ eV). [We have used $J_1 \ll J_2, |J_3|$ again in the derivation of Eq. (82).] In contrast to Eq. (81), the term including $\mathcal{J}_1(u_{ij})^2$ in Eq. (82) gives the positive-sign contribution. Thus, we can see from Eq. (82) that the competition between the negative-sign term including $\mathcal{J}_0(u_{ij})^2$ and the positive-sign term including $\mathcal{J}_1(u_{ij})^2$ is the origin of the sign changes at $|u_{ij}| \sim 0.4, 3.5$ in Fig. 2(b); and that the magnitude changes come from the Bessel functions. Since the leading terms at $\omega = 1.8$ eV is also written in the form of Eq. (82), we can similarly understand the magnitude and sign changes at $\omega = 1.8$ eV. Note that a similar argument is applicable to Eqs. (65), (66), (70)–(72), and (76)–(78).

We turn to the $|u_{ij}|$ dependences of the exchange interactions with linearly polarized light. The $|u_{ij}|$ dependences with $\mathbf{E}_{\text{linear-}b}(t)$ are shown in Figs. 4 and 6, and those with $\mathbf{E}_{\text{linear-}a}(t)$ are shown in Figs. 5 and 7. (Note that the results at $\omega = 1.8$ eV are not shown because they are qualitatively the same as those at $\omega = 2.2$ eV.) Some properties are similar to those with circularly polarized light (Figs. 2 and 3): the sign changes in the exchange interactions are absent at $\omega = 3$ eV and present at $\omega = 2.2$ eV; and the results obtained

in the first case remain qualitatively unchanged even in the second case. The magnitude and sign changes in the exchange interactions can be understood in a way similar to those with circularly polarized light. We also see from Figs. 4–7 that linearly polarized light can change the ratios J_X/J_Z , K_X/K_Z , and Γ_X/Γ_Z even without the bond anisotropy of the hopping integrals. [As explained below Eq. (73), this property results from the difference between u_{ij}^Z and u_{ij}^X .] Because of this property, those ratios can have values which cannot be realized in nondriven α -RuCl₃: although $|J_X| < |J_Z|$, $|K_X| > |K_Z|$, and $\Gamma_X < \Gamma_Z$ hold in nondriven α -RuCl₃, $|J_X| > |J_Z|$, $|K_X| < |K_Z|$, and $\Gamma_X > \Gamma_Z$ are possible in α -RuCl₃ driven by a field of linearly polarized light. In addition, it is possible to change the signs of the exchange interactions only for the Z bonds or only for the X and Y bonds; for example, at $|u_{ij}| \sim 0.5$ in Figs. 4(d)–4(f) we can change the signs for the Z bonds without changing those for the X and Y bonds. Then, the honeycomb-network spin system could be transformed either into weakly coupled zigzag spin chains in the case of $\mathbf{E}_{\text{linear-}b}(t)$ for $|u_{ij}| \approx 0.4$ – 0.42 at $\omega = 2.2$ eV [e.g., see Figs. 4(d)–4(f) and 6(d)–6(f)] or into weakly coupled step spin chains in the case of $\mathbf{E}_{\text{linear-}a}(t)$ for $|u_{ij}| \approx 0.48$ – 0.5 at $\omega = 2.2$ eV [e.g., see Figs. 5(d)–5(f) and 7(d)–7(f)]. In the weakly coupled zigzag spin chains [Fig. 8(a)], $J_X = J_Y$, $K_X = K_Y$, and $\Gamma_X = \Gamma_Y$ are dominant and J_Z , K_Z , and Γ_Z give the weak coupling between zigzag chains; in the weakly coupled step spin chains [Fig. 8(b)], J_Z , K_Z , and Γ_Z are dominant and $J_X = J_Y$, $K_X = K_Y$, and $\Gamma_X = \Gamma_Y$ give the weak coupling between step chains. Note that in the first case of our model with $\mathbf{E}_{\text{linear-}b}(t)$ for $|u_{ij}| \approx 0.42$ at $\omega = 2.2$ eV, $J_X/J_Z \sim 9.8$, $K_X/K_Z \sim 4.6$, and $\Gamma_X/\Gamma_Z \sim 4.6$; and that in the first case with $\mathbf{E}_{\text{linear-}a}(t)$ for

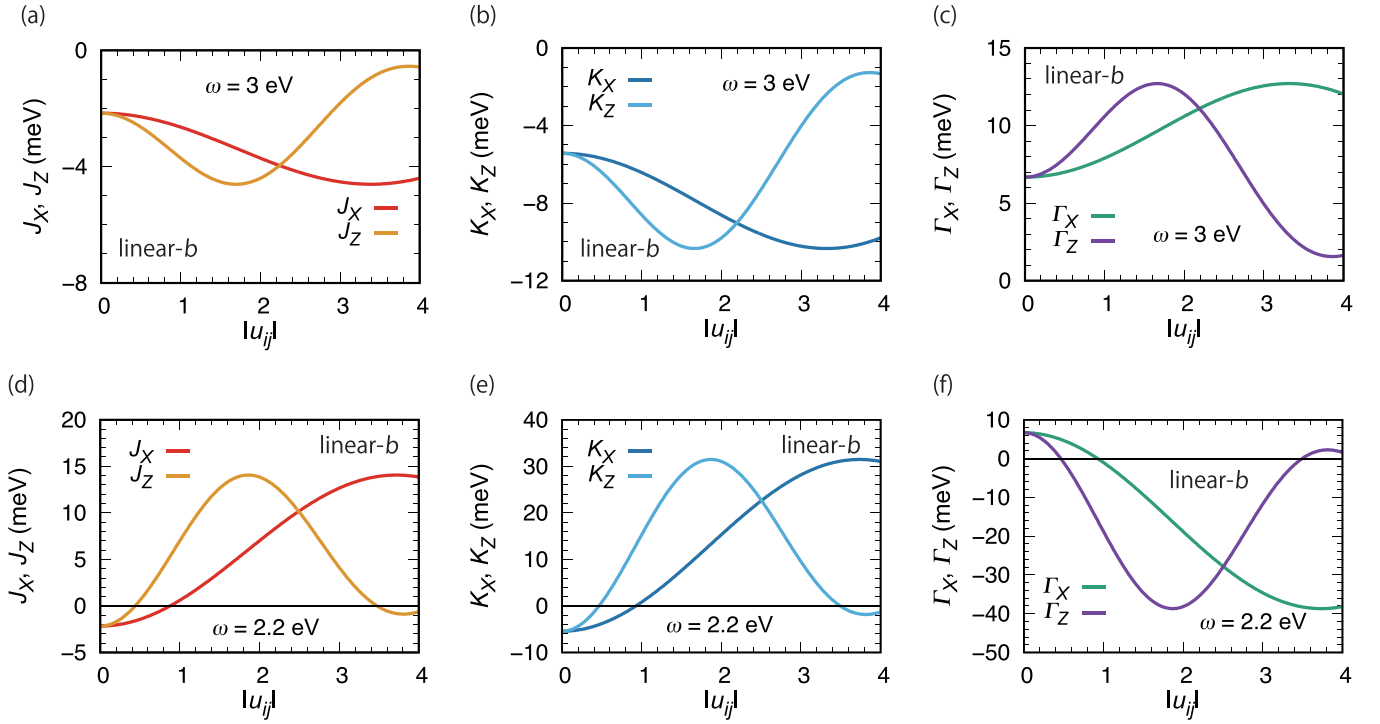


FIG. 4. The $|u_{ij}| (= |\frac{eE_0}{\omega}|)$ dependences of $J_X (=J_Y)$, J_Z , $K_X (=K_Y)$, K_Z , $\Gamma_X (= \Gamma_Y)$, and Γ_Z with $\mathbf{E}_{\text{linear-}b}(t)$ in the first case of our model. The value of ω is 3 eV in (a)–(c) and 2.2 eV in (d)–(f). In contrast to the first case with $\mathbf{E}_{\text{circ}}(t)$ (Fig. 2), the light field induces the bond anisotropy of the exchange interactions even without the bond anisotropy of the hopping integrals.

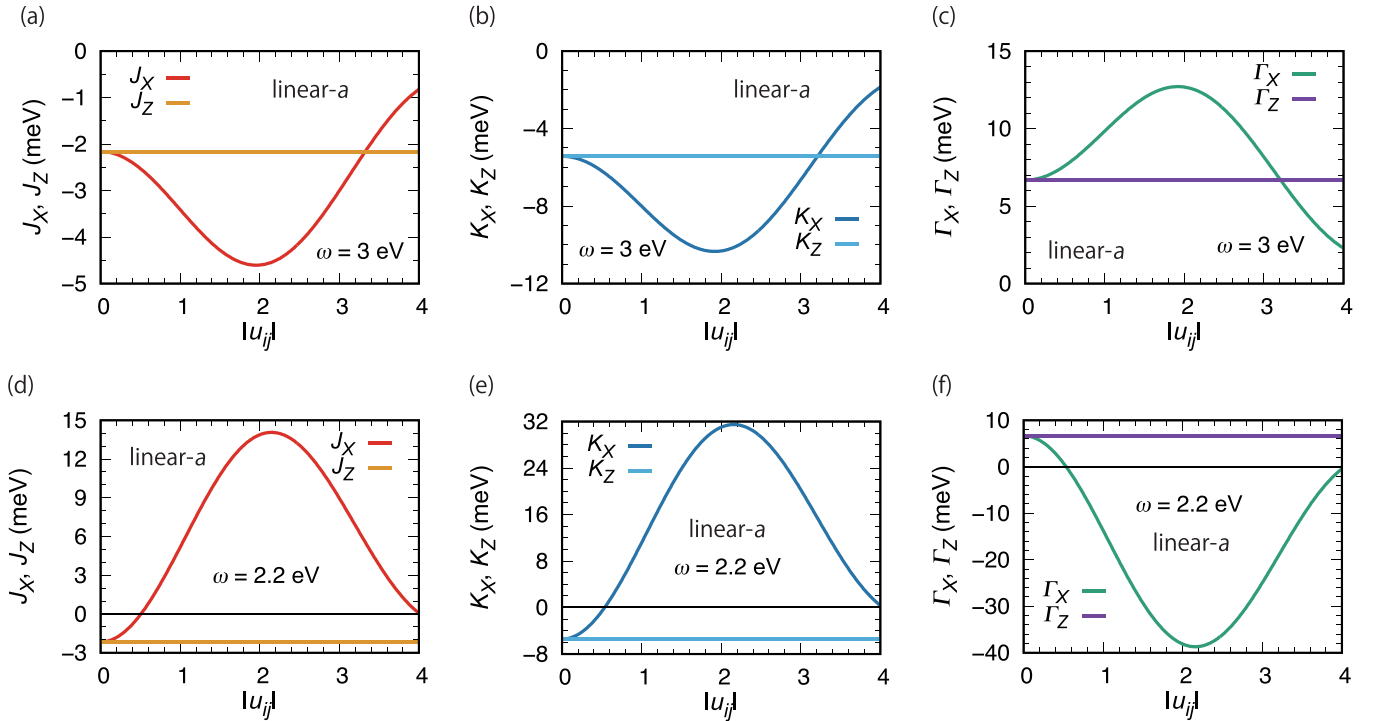


FIG. 5. The $|u_{ij}| (= |\frac{eE_0}{\omega}|)$ dependences of $J_X (=J_Y)$, J_Z , $K_X (=K_Y)$, K_Z , $\Gamma_X (= \Gamma_Y)$, and Γ_Z with $\mathbf{E}_{\text{linear-}a}(t)$ in the first case of our model. The value of ω is 3 eV in (a)–(c) and 2.2 eV in (d)–(f). As well as the first case with $\mathbf{E}_{\text{linear-}b}(t)$ (Fig. 4), the bond anisotropy of the exchange interactions is induced by linearly polarized light; this contrasts with the case with circularly polarized light (Fig. 2). The exchange interactions for the Z bonds are independent of $|u_{ij}|$ because of Eq. (67).

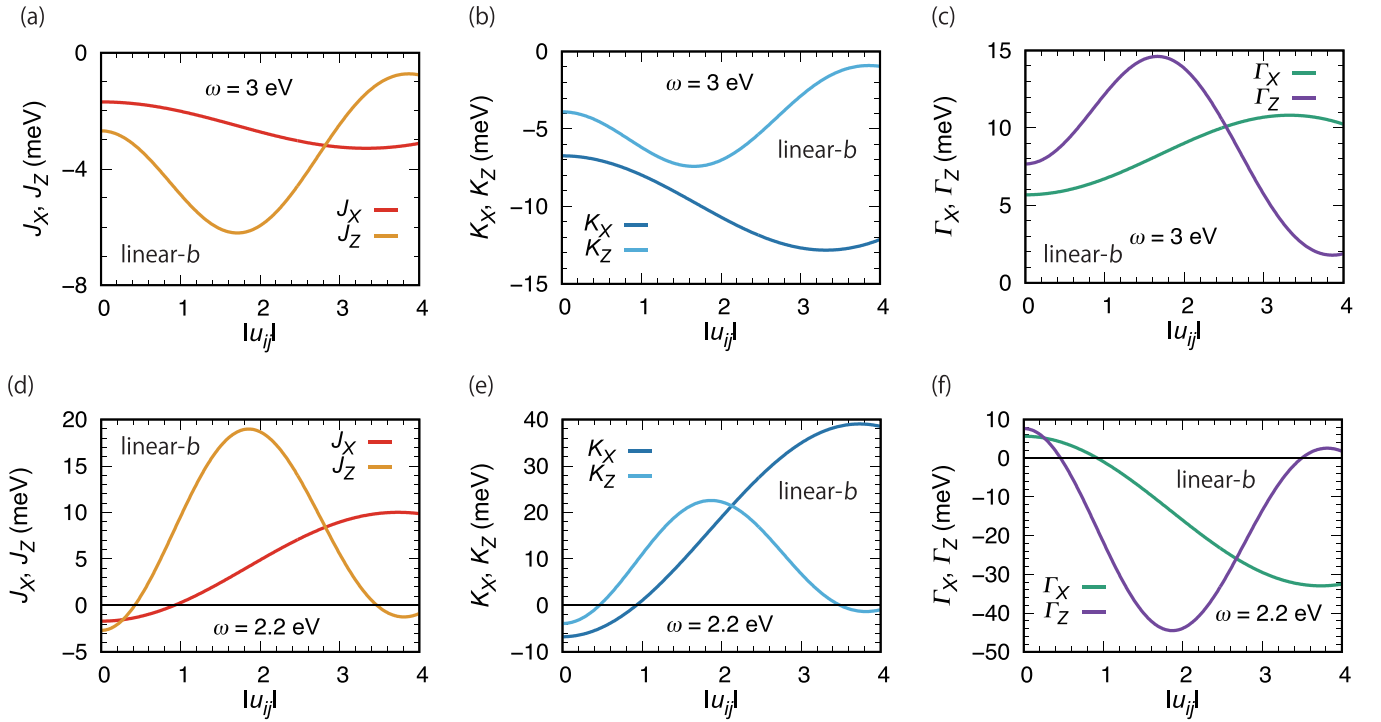


FIG. 6. The $|u_{ij}| (=|\frac{eE_0}{\omega}|)$ dependences of $J_X (=J_Y)$, J_Z , $K_X (=K_Y)$, K_Z , $\Gamma_X (= \Gamma_Y)$, and Γ_Z with $\mathbf{E}_{\text{linear-b}}(t)$ in the second case of our model. The value of ω is 3 eV in (a)–(c) and 2.2 eV in (d)–(f). The bond-anisotropic $|u_{ij}|$ dependences in this case are similar to those obtained in the first case with $\mathbf{E}_{\text{linear-b}}(t)$ (Fig. 4).

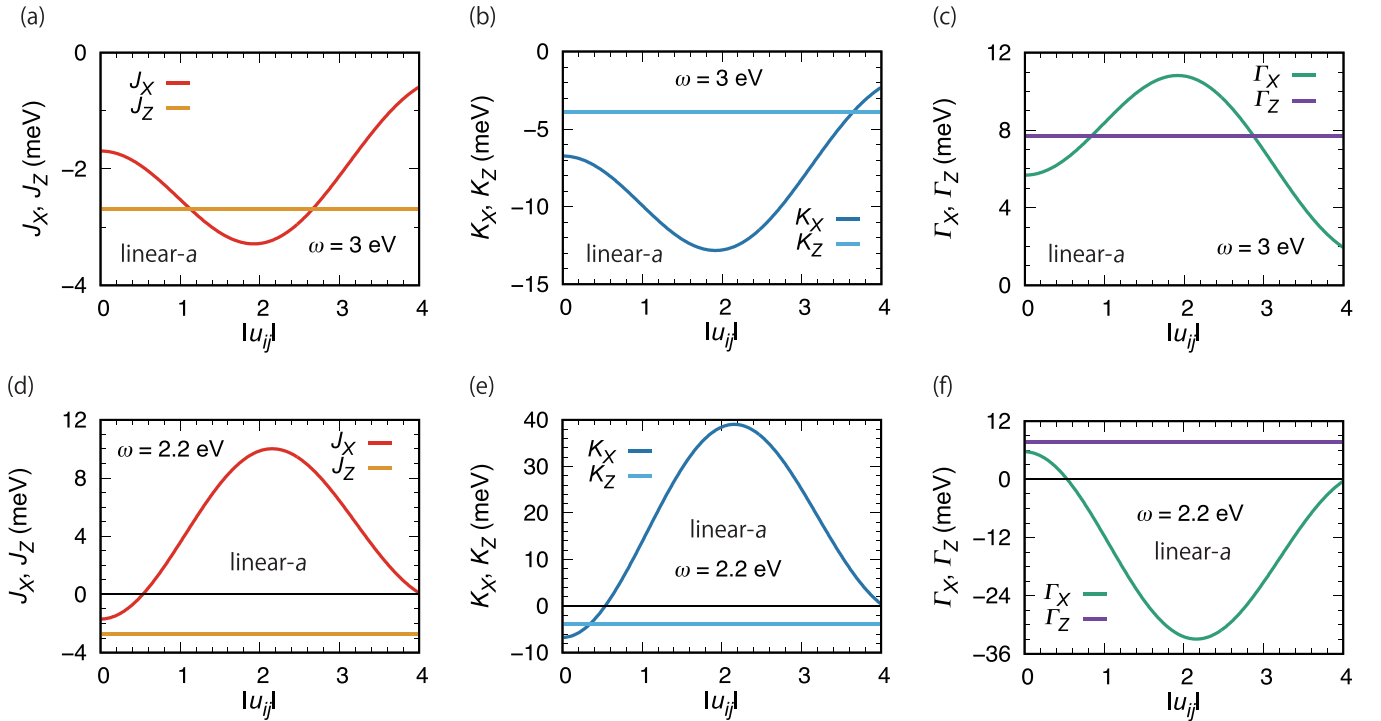


FIG. 7. The $|u_{ij}| (=|\frac{eE_0}{\omega}|)$ dependences of $J_X (=J_Y)$, J_Z , $K_X (=K_Y)$, K_Z , $\Gamma_X (= \Gamma_Y)$, and Γ_Z with $\mathbf{E}_{\text{linear-a}}(t)$ in the second case of our model. The value of ω is 3 eV in (a)–(c) and 2.2 eV in (d)–(f). As well as the case with $\mathbf{E}_{\text{linear-b}}(t)$, the bond-anisotropic $|u_{ij}|$ dependences in this case are similar to those obtained in the first case with $\mathbf{E}_{\text{linear-a}}(t)$ (Fig. 5).

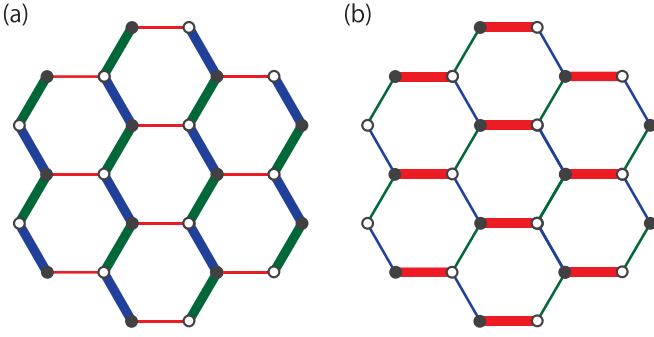


FIG. 8. Weakly coupled (a) zigzag and (b) step spin chains with $E_{\text{linear-}b}(t)$ and $E_{\text{linear-}a}(t)$, respectively. The definitions of blue, green, and red lines and black and white circles are the same as those in Fig. 1. Thicker bonds represent the bonds with the exchange interactions which are larger in magnitude.

$|u_{ij}| \approx 0.48$ at $\omega = 2.2$ eV, $J_X/J_Z \sim 0.1$, $K_X/K_Z \sim 0.2$, and $\Gamma_X/\Gamma_Z \sim 0.2$.

IV. MAGNETIC STATES

In this section, we study several magnetic states in periodically driven α -RuCl₃. In Sec. IV A, we evaluate the expectation value of our Floquet Hamiltonian within the MFA and express it in a quadratic form. Then, we explain how to obtain the energies and spin configurations of magnetic states. We also remark on the magnetic states considered in our analyses. In Sec. IV B, we present the $|u_{ij}|$ dependences of the energies of the magnetic states for some nonresonant ω 's and discuss the effects of one of the light fields and the differences due to the polarization of light. (The reason why we use nonresonant ω 's has been explained in Sec. III.)

A. Theory

Applying the MFA to our Floquet Hamiltonian, we derive an expression of its expectation value in a quadratic form. Since the MFA for Mott insulators with strong SOC has been explained, for example, in Ref. [14], we explain the main points here. By using the MFA, we can write the expectation value of Eq. (74) as

$$\langle \bar{H}_{\text{eff}} \rangle = \sum_{\langle i,j \rangle} \sum_{\mu, \nu=x,y,z} M_{\mu\nu}^{ij} \langle S_i^\mu \rangle \langle S_j^\nu \rangle, \quad (83)$$

where $M_{\mu\nu}^{ij}$ is given in the first or second case of our model by

$$M_{\mu\nu}^{ij} = \begin{cases} J_\delta + K_\delta & (\mu = \nu = \gamma), \\ J_\delta & (\mu = \nu = \alpha \text{ or } \beta), \\ \Gamma_\delta & (\mu = \alpha, \nu = \beta), \\ \Gamma_\delta & (\mu = \beta, \nu = \alpha), \\ 0 & (\text{otherwise}). \end{cases} \quad (84)$$

[Note that δ , γ , α , and β have been defined in Eq. (75).] In the third, fourth, or fifth case of our model, the contribution from Eq. (79) is added to Eq. (83). In the MFA, the expectation value of spin operators should satisfy the hard-spin constraints:

$$|\langle S_i \rangle|^2 = S^2, \quad |\langle S_j \rangle|^2 = S^2, \quad (85)$$

where i and j belong to the A and the B sublattices (Fig. 1), respectively, and S is 1/2 in the case of α -RuCl₃. Since $\langle S_i^\mu \rangle$ and $\langle S_j^\nu \rangle$ are expressed as

$$\langle S_i^\mu \rangle = \sqrt{\frac{2}{N}} \sum_{\mathbf{q}} \langle S_{qA}^\mu \rangle e^{i\mathbf{q} \cdot \mathbf{R}_i}, \quad (86)$$

$$\langle S_j^\nu \rangle = \sqrt{\frac{2}{N}} \sum_{\mathbf{q}} \langle S_{qB}^\nu \rangle e^{i\mathbf{q} \cdot \mathbf{R}_j}, \quad (87)$$

where N is the total number of sites, we can express Eq. (83) in the following quadratic form:

$$\begin{aligned} \langle \bar{H}_{\text{eff}} \rangle &= \sum_{\mathbf{q}} \sum_{\mu, \nu=x,y,z} \sum_{l, l'=A,B} \langle S_{ql}^\mu \rangle^* [M_{ll'}(\mathbf{q})]_{\mu\nu} \langle S_{ql'}^\nu \rangle \\ &= \sum_{\mathbf{q}} \sum_{\mu, \nu=x,y,z} \langle S_{-qA}^\mu \rangle [M(\mathbf{q})]_{\mu\nu} \langle S_{qB}^\nu \rangle \\ &\quad + \sum_{\mathbf{q}} \sum_{\mu, \nu=x,y,z} \langle S_{-qB}^\mu \rangle [M(\mathbf{q})^\dagger]_{\mu\nu} \langle S_{qA}^\nu \rangle, \end{aligned} \quad (88)$$

where the $\mu \times \nu$ matrix $M(\mathbf{q})$ is given by the matrix

$$\begin{pmatrix} J(\mathbf{q}) + K_x(\mathbf{q}) & \Gamma_z(\mathbf{q}) & \Gamma_y(\mathbf{q}) \\ \Gamma_z(\mathbf{q}) & J(\mathbf{q}) + K_y(\mathbf{q}) & \Gamma_x(\mathbf{q}) \\ \Gamma_y(\mathbf{q}) & \Gamma_x(\mathbf{q}) & J(\mathbf{q}) + K_z(\mathbf{q}) \end{pmatrix}, \quad (89)$$

and $J(\mathbf{q})$, $K_\mu(\mathbf{q})$'s, and $\Gamma_\mu(\mathbf{q})$'s are defined as

$$\begin{aligned} J(\mathbf{q}) &= \frac{J_X}{2} e^{-i\frac{q_x}{2} + i\frac{\sqrt{3}}{2}q_y} + \frac{J_Y}{2} e^{-i\frac{q_x}{2} - i\frac{\sqrt{3}}{2}q_y} + \frac{J_Z}{2} e^{iq_x} \\ &\quad + \frac{J_X^{\text{3rd}}}{2} e^{iq_x - i\sqrt{3}q_y} + \frac{J_Y^{\text{3rd}}}{2} e^{iq_x + i\sqrt{3}q_y} + \frac{J_Z^{\text{3rd}}}{2} e^{-2iq_x}, \end{aligned} \quad (90)$$

$$K_x(\mathbf{q}) = \frac{K_X}{2} e^{-i\frac{q_x}{2} + i\frac{\sqrt{3}}{2}q_y}, \quad (91)$$

$$K_y(\mathbf{q}) = \frac{K_Y}{2} e^{-i\frac{q_x}{2} - i\frac{\sqrt{3}}{2}q_y}, \quad (92)$$

$$K_z(\mathbf{q}) = \frac{K_Z}{2} e^{iq_x}, \quad (93)$$

$$\Gamma_x(\mathbf{q}) = \frac{\Gamma_X}{2} e^{-i\frac{q_x}{2} + i\frac{\sqrt{3}}{2}q_y}, \quad (94)$$

$$\Gamma_y(\mathbf{q}) = \frac{\Gamma_Y}{2} e^{-i\frac{q_x}{2} - i\frac{\sqrt{3}}{2}q_y}, \quad (95)$$

$$\Gamma_z(\mathbf{q}) = \frac{\Gamma_Z}{2} e^{iq_x}. \quad (96)$$

The details of the derivation of Eq. (88) are described in Appendix E. Furthermore, we make some remarks about momentum in the case of the honeycomb lattice in Appendix F. Note that the MFA can reproduce the phase diagram obtained in the Luttinger-Tizsa method [28,29] [i.e., Fig. 2(a) of Ref. [12] except the region surrounded by the dashed white line [30]].

By using Eqs. (85)–(96), we can obtain the energies and spin configurations of magnetic states. Since Eq. (88) is quadratic in spin variables, we obtain six eigenvalues and the corresponding eigenvectors for each \mathbf{q} by diagonalizing the matrix

$$\begin{pmatrix} 0 & M(\mathbf{q}) \\ M(\mathbf{q})^\dagger & 0 \end{pmatrix}, \quad (97)$$

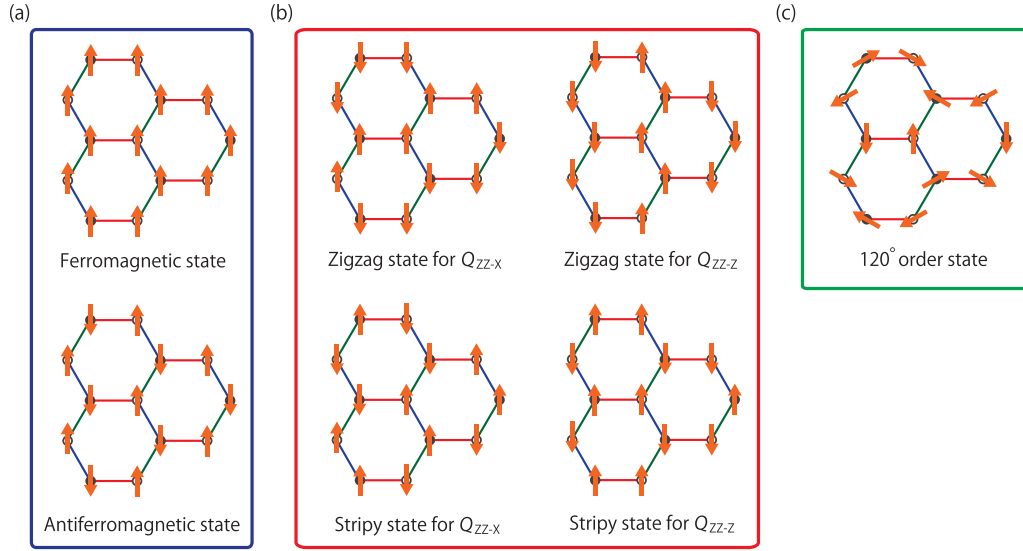


FIG. 9. Spin configurations of the magnetic states considered in our analyses: (a) the magnetic states with $\mathbf{Q} = \mathbf{0}$, the ferromagnetic state and the antiferromagnetic state, (b) the magnetic states with $\mathbf{Q} = \mathbf{Q}_{ZZ-X} (= \mathbf{K}_{01}/2)$ or $\mathbf{Q} = \mathbf{Q}_{ZZ-Z} (= \mathbf{K}_{10}/2)$, the zigzag states and the stripy states, and (c) the magnetic state with $\mathbf{Q} = \mathbf{Q}_{120}$, the 120° order state. Specific directions of spins, which are represented by the arrows, are chosen because the relative angles between the neighboring spins are essential for understanding the differences in the spin configurations.

where $M(\mathbf{q})$ has been defined in Eq. (89) and 0 represents the zero matrix (i.e., the $\mu \times \nu$ matrix of which the components are all zero). At a certain \mathbf{q} , for example $\mathbf{q} = \mathbf{Q}$, the eigenvalue which is the smallest of the six ones gives the energy of a magnetic state characterized by the ordering vector \mathbf{Q} . Then, its spin configuration can be obtained by combining the corresponding eigenvectors and Eqs. (85)–(87); the obtained spin configuration is valid only if it is consistent with Eq. (85).

In the analyses of Sec. IV B, we consider several magnetic states, which can be classified into three groups. The first group consists of the magnetic states with $\mathbf{Q} = \mathbf{0}$, which include a ferromagnetic state and an antiferromagnetic state [Fig. 9(a)]. Note that the \mathbf{Q} of the antiferromagnetic state becomes $\mathbf{0}$ in the presence of a sublattice structure (because of it, the spins on a sublattice are all ferromagnetic, i.e., parallel). The second group consists of the magnetic states with $\mathbf{Q} = \mathbf{K}/2$, where \mathbf{K} is the reciprocal lattice vector [Eq. (F6)]; they include the zigzag states and the stripy states [Fig. 9(b)]. If we see a unit consisting of one site on the A or B sublattice and its three neighbors, in the zigzag states three spins are ferromagnetic (parallel) and the other is antiferromagnetic (antiparallel); in the stripy states two spins are ferromagnetic and the others are antiferromagnetic [Fig. 9(b)]. In our analyses, we consider two kinds of $\mathbf{Q} = \mathbf{K}/2$, i.e., one is $\mathbf{Q}_{ZZ-X} = \mathbf{K}_{01}/2$ and the other is $\mathbf{Q}_{ZZ-Z} = \mathbf{K}_{10}/2$ (for the details of \mathbf{K}_{01} and \mathbf{K}_{10} , see Appendix F). In the zigzag state with $\mathbf{Q} = \mathbf{Q}_{ZZ-X}$ or $\mathbf{Q} = \mathbf{Q}_{ZZ-Z}$ the spins on the X or the Z bonds, respectively, are antiferromagnetic; in the stripy state with $\mathbf{Q} = \mathbf{Q}_{ZZ-X}$ or $\mathbf{Q} = \mathbf{Q}_{ZZ-Z}$ those are ferromagnetic. This difference between the zigzag (or stripy) states with $\mathbf{Q} = \mathbf{Q}_{ZZ-X}$ and \mathbf{Q}_{ZZ-Z} is partly due to the momentum dependences of $K_\mu(\mathbf{q})$'s. Namely, since Eqs. (91)–(93) show

$$K_x(\mathbf{Q}_{ZZ-X}) = \frac{K_X}{2} e^{i\pi} e^{-i\pi/3} = \frac{-K_X}{2} e^{-i\pi/3}, \quad (98)$$

$$K_y(\mathbf{Q}_{ZZ-X}) = \frac{K_Y}{2} e^{-i\pi/3}, \quad (99)$$

$$K_z(\mathbf{Q}_{ZZ-X}) = \frac{K_Z}{2} e^{-i\pi/3}, \quad (100)$$

and

$$K_x(\mathbf{Q}_{ZZ-Z}) = \frac{K_X}{2} e^{-i\pi/3}, \quad (101)$$

$$K_y(\mathbf{Q}_{ZZ-Z}) = \frac{K_Y}{2} e^{-i\pi/3}, \quad (102)$$

$$K_z(\mathbf{Q}_{ZZ-Z}) = \frac{K_Z}{2} e^{i\pi} e^{-i\pi/3} = \frac{-K_Z}{2} e^{-i\pi/3}, \quad (103)$$

the effective Kitaev interaction of the X bonds for $\mathbf{Q} = \mathbf{Q}_{ZZ-X}$ or of the Z bonds for $\mathbf{Q} = \mathbf{Q}_{ZZ-Z}$ has the opposite sign and, as a result, the spins on the X bonds for $\mathbf{Q} = \mathbf{Q}_{ZZ-X}$ or the Z bonds for $\mathbf{Q} = \mathbf{Q}_{ZZ-Z}$ are aligned in the opposite direction compared with the spins on the other bonds. The third group consists of the magnetic state with $\mathbf{Q} = \mathbf{Q}_{120}$, the 120° order state [Fig. 9(c)]. The magnetic states explained above are realized in Mott insulators with strong SOC on the honeycomb lattice [12,15].

B. Results

To study how the light fields affect the magnetic states, we numerically calculate their energies within the MFA in the five cases of our model at $\omega = 3$ and 2.2 eV. (The results at $\omega = 1.8$ eV, which are not shown, are qualitatively the same as those at $\omega = 2.2$ eV.) As explained in Sec. IV A, the energy of a magnetic state characterized by \mathbf{Q} corresponds to the lowest eigenvalue obtained by diagonalizing Eq. (97) at $\mathbf{q} = \mathbf{Q}$. Furthermore, the \mathbf{Q} 's considered in this study are $\mathbf{0}$, $\mathbf{Q}_{ZZ-X} (= \mathbf{K}_{01}/2)$, $\mathbf{Q}_{ZZ-Z} (= \mathbf{K}_{10}/2)$, and \mathbf{Q}_{120} . In the numerical calculations, we impose the periodic boundary condition and set $N_1 = N_2 = 120$ in Eq. (F5). The parameters of our model except t_{3rd} are chosen in the way described in Sec. III B. We

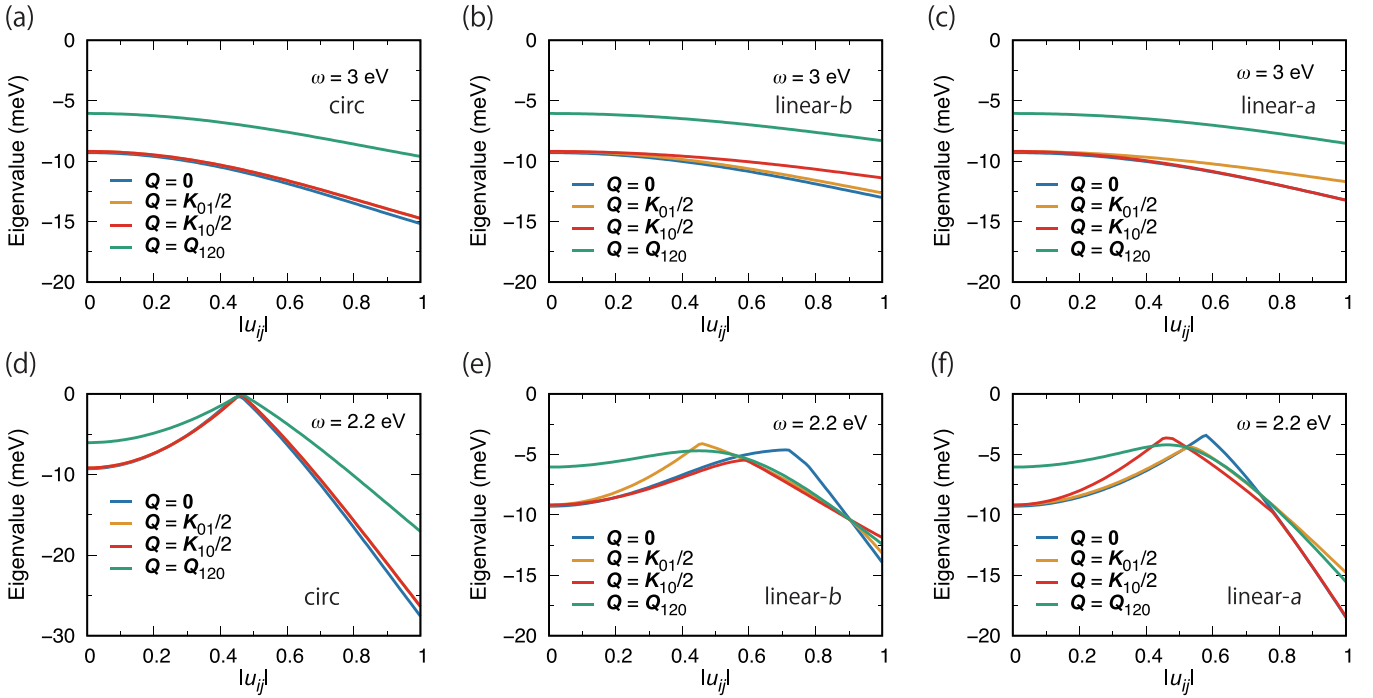


FIG. 10. The $|u_{ij}|$ dependences of the energies of the magnetic states for $\mathbf{Q} = \mathbf{0}$, $\mathbf{Q}_{ZZ-X}(=K_{01}/2)$, $\mathbf{Q}_{ZZ-Z}(=K_{10}/2)$, and \mathbf{Q}_{120} within the MFA in the first case of our model with $\mathbf{E}_{\text{circ}}(t)$ [(a) and (d)], $\mathbf{E}_{\text{linear-b}}(t)$ [(b) and (e)], and $\mathbf{E}_{\text{linear-a}}(t)$ [(c) and (f)]. The value of ω is 3 eV in (a)–(c) and 2.2 eV in (d)–(f). In this case, the bond-averaged nearest-neighbor hopping integrals are considered.

set $t_{3\text{rd}} = -40$ meV in the third or fourth case and $t_{3\text{rd}} = -60$ meV in the fifth case. Note that the former value corresponds to the average of the intraorbital hopping integral of the d_{xy} orbital for the Z_3 bonds, that of the d_{yz} orbital for the X_3 bonds, and that of the d_{xz} orbital for the Y_3 bonds which are obtained in the first-principles calculations [13]; and that the latter value is also considered to clarify the effects of $J_{\delta}^{3\text{rd}}$ in detail.

Before discussing the properties for $|u_{ij}| \neq 0$, we comment on the properties at $u_{ij} = 0$ in the five cases of our model. First, the ferromagnetic state, a magnetic state with $\mathbf{Q} = \mathbf{0}$, has the lowest energy in the first, second, and fourth cases, whereas the zigzag state for $\mathbf{Q} = \mathbf{Q}_{ZZ-Z}$, a magnetic state with $\mathbf{Q} = K_{10}/2$, is the lowest-energy state in the third and fifth cases; the 120° order state has the highest energy in all the cases. This result indicates that the stability of the zigzag or ferromagnetic state is sensitive to the value of $t_{3\text{rd}}$ and the degree of the bond anisotropy of the hopping integrals. Since the main effect of $t_{3\text{rd}}$ is to induce $J_{\delta}^{3\text{rd}}$, our result is consistent with the result obtained in a minimal model of α -RuCl₃ [13]. Furthermore, the competition between these magnetic states agrees with the experimental result [31]. The sensitivity to $J_{\delta}^{3\text{rd}}$ can be understood by estimating its energy in the MFA: since the expectation value of Eq. (79) can be written in the MFA as $\sum_{\langle\langle(i,j)\rangle\rangle} J_{\delta}^{3\text{rd}} \langle S_i \rangle \cdot \langle S_j \rangle$, the corresponding energies per spin surrounded by three third neighbors for the ferromagnetic, zigzag, and 120° order states are $3J_{3\text{rd}}S^2$, $-3J_{3\text{rd}}S^2$, and 0, respectively, where $J_X^{3\text{rd}} = J_Y^{3\text{rd}} = J_Z^{3\text{rd}} = J_{3\text{rd}}$. Then, the zigzag states for $\mathbf{Q} = \mathbf{Q}_{ZZ-Z}$ and \mathbf{Q}_{ZZ-X} , ones of the magnetic states with $\mathbf{Q} = K_{10}/2$ and $K_{01}/2$, are degenerate in the first and third cases; in the second, fourth, and fifth cases, this degeneracy is lifted and the former state is of lower energy.

This lifting is due to the bond anisotropy of the hopping integrals; in addition, the lower energy of the zigzag state for $\mathbf{Q} = \mathbf{Q}_{ZZ-Z}$ is mainly due to $|J_X + K_X| > |J_Z + K_Z|$, which makes the ferromagnetic spin alignment of the X bonds more stable than that of the Z bonds. (As explained in Sec. IV A, two spins on a X or Z bond are antiferromagnetic in the zigzag state for $\mathbf{Q} = \mathbf{Q}_{ZZ-X}$ or \mathbf{Q}_{ZZ-Z} , respectively.) Note that the energy difference between these zigzag states is about 0.1 meV per spin.

We now present the $|u_{ij}|$ dependences of the energies of the magnetic states in the first case of our model with $\mathbf{E}_{\text{circ}}(t)$, $\mathbf{E}_{\text{linear-b}}(t)$, or $\mathbf{E}_{\text{linear-a}}(t)$. These dependences at $\omega = 3$ and 2.2 eV are shown in Fig. 10. The results with $\mathbf{E}_{\text{circ}}(t)$ [Figs. 10(a) and 10(d)] show that the energies of the magnetic states with $\mathbf{Q} = \mathbf{0}$, \mathbf{Q}_{ZZ-X} , and \mathbf{Q}_{ZZ-Z} are close even in the range of $0 < |u_{ij}| \leq 1$ and that the energy of the 120° order state is much higher than them except near the $|u_{ij}|$'s at which the exchange interactions are very small in magnitude [see Figs. 2(b) and 10(d)]. The similar properties hold even in the results with $\mathbf{E}_{\text{linear-b}}(t)$ or $\mathbf{E}_{\text{linear-a}}(t)$ at $\omega = 3$ eV [Fig. 10(b) or 10(c)].

There are several properties characteristic of the linearly polarized light fields. One is the lifting of the degeneracy of the magnetic states with $\mathbf{Q} = \mathbf{Q}_{ZZ-X}$ and \mathbf{Q}_{ZZ-Z} . For example, in the case with $\mathbf{E}_{\text{linear-b}}(t)$ at $\omega = 3$ eV the magnetic state with $\mathbf{Q} = \mathbf{Q}_{ZZ-X}$ is of lower energy than that with $\mathbf{Q} = \mathbf{Q}_{ZZ-Z}$ [Fig. 10(b)], whereas in the case with $\mathbf{E}_{\text{linear-a}}(t)$ at $\omega = 3$ eV the latter is of lower energy [Fig. 10(c)]. This lifting is due to the light-induced bond anisotropy of the exchange interactions, one of the characteristics of linearly polarized light. The property that the magnetic state with $\mathbf{Q} = \mathbf{Q}_{ZZ-X}$ is of lower energy than that with $\mathbf{Q} = \mathbf{Q}_{ZZ-Z}$ in the case with $\mathbf{E}_{\text{linear-b}}(t)$ at

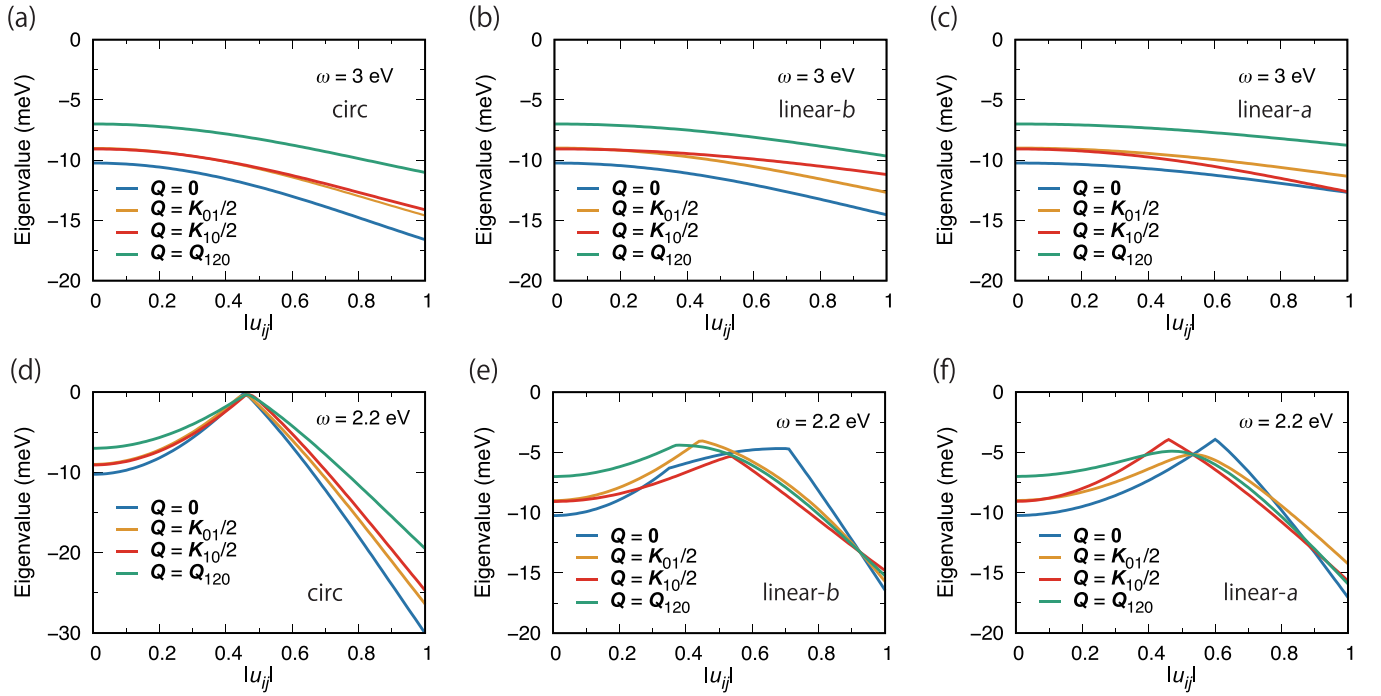


FIG. 11. The $|u_{ij}|$ dependences of the energies of the magnetic states for $\mathbf{Q} = \mathbf{0}$, $\mathbf{Q}_{ZZ-X}(=\mathbf{K}_{01/2})$, $\mathbf{Q}_{ZZ-Z}(=\mathbf{K}_{10/2})$, and \mathbf{Q}_{120} within the MFA in the second case of our model with $E_{\text{circ}}(t)$ [(a) and (d)], $E_{\text{linear-b}}(t)$ [(b) and (e)], and $E_{\text{linear-a}}(t)$ [(c) and (f)]. The value of ω is 3 eV in (a)–(c) and 2.2 eV in (d)–(f). In this case, the bond-anisotropic nearest-neighbor hopping integrals are considered. In contrast to the first case (Fig. 10), the degeneracy of the magnetic states for $\mathbf{Q} = \mathbf{K}_{01/2}$ and $\mathbf{K}_{10/2}$ is lifted even for $E_{\text{circ}}(t)$ due to the bond anisotropy of the nearest-neighbor hopping integrals.

$\omega = 3$ eV comes from the facts that the exchange interactions for the Z bonds are larger in magnitude than those for the X or Y bonds and that J_Z and K_Z are ferromagnetic [see Figs. 4(a)–4(c) in the range of $0 \leq |u_{ij}| \leq 1$]; the property in the case with $E_{\text{linear-a}}(t)$ at $\omega = 3$ eV can be similarly understood. The other characteristic properties are the changes in the competing magnetic states. From Fig. 10(e), we see the competing magnetic states in the range of $0 < |u_{ij}| \leq 0.4$ are the magnetic states with $\mathbf{Q} = \mathbf{0}$ and \mathbf{Q}_{ZZ-Z} , whereas those in the range of $0.6 \leq |u_{ij}| \leq 0.8$ become the magnetic states with $\mathbf{Q} = \mathbf{Q}_{ZZ-Z}$, \mathbf{Q}_{ZZ-X} , and \mathbf{Q}_{120} . In addition, from Fig. 10(f), we see a similar change in the competing magnetic states. These results are related to the light-induced bond anisotropy of the exchange interactions because in the range of $0.6 \leq |u_{ij}| \leq 0.8$ with $E_{\text{linear-b}}(t)$ or $E_{\text{linear-a}}(t)$ the signs of the exchange interactions only for the Z bonds or for the X and Y bonds, respectively, are changed and their magnitudes become larger than those for the other bonds [see Figs. 4(d)–4(f) for $E_{\text{linear-b}}(t)$ and Figs. 5(d)–4(f) for $E_{\text{linear-a}}(t)$].

We turn to the results in the second case of our model. Figure 11 shows the $|u_{ij}|$ dependences of the energies of the magnetic states in this case with $E_{\text{circ}}(t)$, $E_{\text{linear-b}}(t)$, or $E_{\text{linear-a}}(t)$. These results are qualitatively the same as those in the first case except that the degeneracy of the magnetic states with $\mathbf{Q} = \mathbf{Q}_{ZZ-X}$ and \mathbf{Q}_{ZZ-Z} is lifted even for $E_{\text{circ}}(t)$. (As described above, this lifting results from the bond anisotropy of the hopping integrals, which is absent in the first case and present in the second case.) Combining this result with the results at $u_{ij} = 0$, we find that the main effects of the bond anisotropy of the hopping integrals are to lift the degeneracy

of the magnetic states with $\mathbf{Q} = \mathbf{Q}_{ZZ-X}$ and \mathbf{Q}_{ZZ-Z} and to decrease the energy of the ferromagnetic state compared with those of the zigzag states at $u_{ij} = 0$.

As well as the results in the second cases, the results in the third case (Fig. 12) are similar to those in the first case except for two differences. The two differences are that at $u_{ij} = 0$ the energies of the zigzag states are lower than that of the ferromagnetic state and that the magnetic state with $\mathbf{q} = \mathbf{0}$ becomes of lower energy than those of the magnetic states with $\mathbf{Q} = \mathbf{Q}_{ZZ-X}$ and \mathbf{Q}_{ZZ-Z} above a certain value of $|u_{ij}|$ [e.g., see the values at $|u_{ij}| = 0.46$ in Fig. 12(a)]. These differences result from the effects of $J_{\delta}^{3\text{rd}}$ because the latter difference can be understood from the $|u_{ij}|$ dependences of $J_{\delta}^{3\text{rd}}$ (Fig. 13); for example, in the case with $E_{\text{circ}}(t)$ at $\omega = 3$ eV the blue and red lines of Fig. 12(a) cross at the value of $|u_{ij}|$ at which $J_{3\text{rd}}$ is small in magnitude [Fig. 13(a)]. Then, as described above, the former difference can be understood from the difference in the energies due to $J_{\delta}^{3\text{rd}}$.

The similar effects of $J_{\delta}^{3\text{rd}}$ appear in the fourth and fifth cases (Figs. 14 and 15). However, in the presence of the bond anisotropy of the nearest-neighbor hopping integrals $t_{3\text{rd}} = -40$ meV is not sufficient for making the energies of the zigzag states lower at $u_{ij} = 0$ than that of the ferromagnetic state (Fig. 14), although the zigzag states are of lower energy at $u_{ij} = 0$ for $t_{3\text{rd}} = -60$ meV (Fig. 15). Nevertheless, we believe this does not contradict the experimental result that the zigzag state is stabilized in α -RuCl₃ because $J_{\delta}^{3\text{rd}}$ is underestimated in our simplified treatment (see Sec. III A and Appendix D); a more accurate calculation is beyond the scope of this paper.

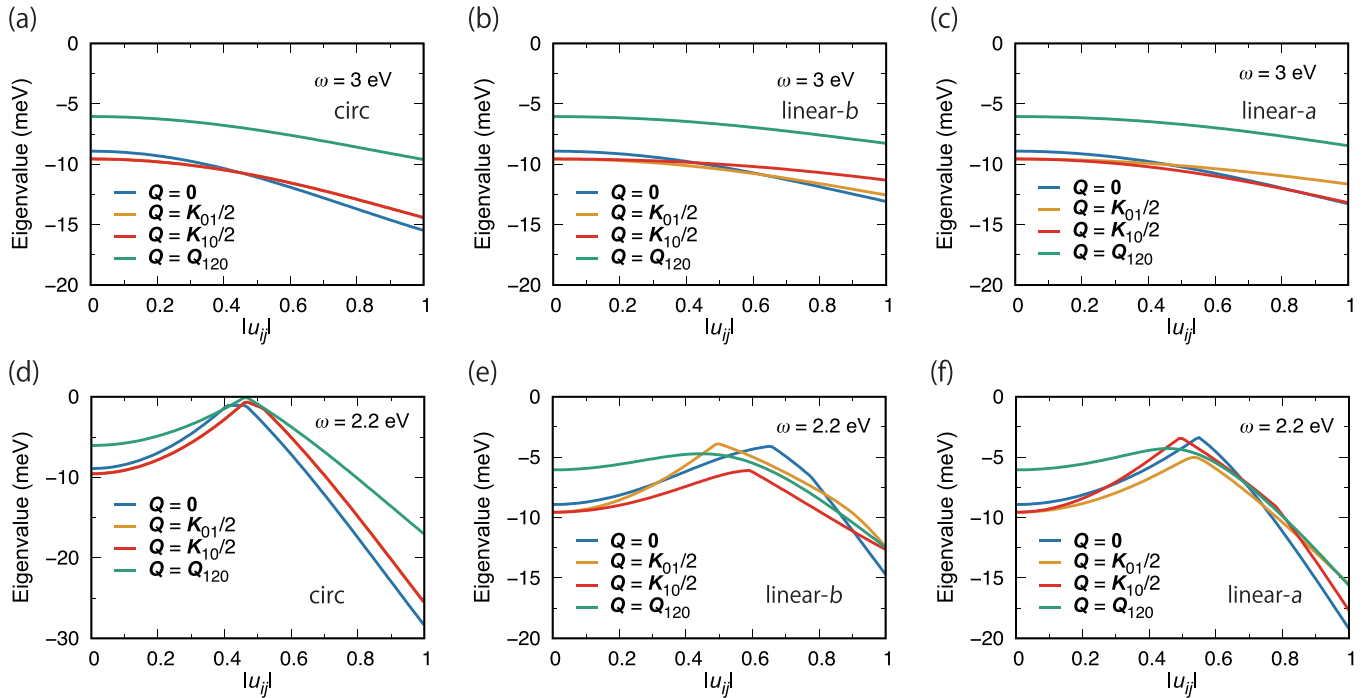


FIG. 12. The $|u_{ij}|$ dependences of the energies of the magnetic states for $\mathbf{Q} = \mathbf{0}$, $\mathbf{Q}_{ZZ-X}(=\mathbf{K}_{01/2})$, $\mathbf{Q}_{ZZ-Z}(=\mathbf{K}_{10/2})$, and \mathbf{Q}_{120} within the MFA in the third case of our model with $\mathbf{E}_{\text{circ}}(t)$ [(a) and (d)], $\mathbf{E}_{\text{linear-b}}(t)$ [(b) and (e)], and $\mathbf{E}_{\text{linear-a}}(t)$ [(c) and (f)]. The value of ω is 3 eV in (a)–(c) and 2.2 eV in (d)–(f). In this case, the bond-averaged nearest-neighbor hopping integrals and the third-neighbor one are considered. In contrast to the first case (Fig. 10), the magnetic state for $\mathbf{Q} = \mathbf{K}_{01/2}$ or $\mathbf{K}_{10/2}$ has the lower energy than that for $\mathbf{Q} = \mathbf{0}$ owing to finite $J_{\delta}^{3\text{rd}}$ induced by the third-neighbor hopping integral.

The most important thing seen from Figs. 11, 12, 14, and 15 is that the characteristic properties found in the first case remain qualitatively unchanged even in the other four cases. Thus, we believe the lifting of the magnetic states with $\mathbf{Q} = \mathbf{Q}_{ZZ-X}$ and \mathbf{Q}_{ZZ-Z} and the change in the competing magnetic states are characteristic of linearly polarized light. Although the former can be realized by using the bond-anisotropic nearest-neighbor hopping integrals, the latter is a unique effect of linearly polarized light.

V. DISCUSSION

First, we discuss the validity of our model. Our model has the three nearest-neighbor hopping integrals, including their bond anisotropy, and the third-neighbor one. For the Mott insulating state, the effective Hamiltonian consists of the nearest-neighbor Heisenberg, Kitaev, and off-diagonal symmetric exchange interactions and the third-neighbor Heisenberg interaction (i.e., J_{δ} , K_{δ} , Γ_{δ} , and $J_{\delta}^{3\text{rd}}$). We believe our model is sufficient for describing the magnetic properties of α -RuCl₃ because its first-principles calculations [13] showed that the leading hopping integrals are t_2 and t_3 , which are at least an order of magnitude larger than the others, and suggested that its minimal spin model consists of the bond-averaged J_{δ} , K_{δ} , $\Gamma_{\delta}(=-K_{\delta})$, and $J_{\delta}^{3\text{rd}}$. In addition, the signs of the exchange interactions of our model are consistent with those estimated by fitting a magnetization measurement [32]. Note that according to this measurement, another off-diagonal symmetric exchange interaction Γ' , which does not appear in our model, is smaller than these four exchange interactions.

The similar results are obtained in other studies [13,31]. This is reasonable because Γ' is proportional to the other nearest-neighbor interorbital hopping integral [12], which is small in the case of α -RuCl₃ [13].

We should note that although the effect of SOC on the coefficients of the exchange interactions is necessary for discussing their values quantitatively [13], the following arguments indicate that its effect may be not large in the case of α -RuCl₃. In general, H_{SOC} affects the coefficients of the exchange interactions of Mott insulators, as we can see from Eq. (55). Since the LS -type SOC induces the onsite interorbital excitations, it can connect $|i; \Gamma, g_{\Gamma}\rangle$ with $|i; \Gamma, g'_{\Gamma}\rangle$ for $g'_{\Gamma} \neq g_{\Gamma}$; such off-diagonal terms result in the degeneracy lifting of the states $|i; \Gamma, g_{\Gamma}\rangle$'s for given Γ . Thus, the main effect of H_{SOC} on the coefficients of the exchange interactions is to change the energies of the intermediate states in the second-order perturbation processes considered to derive the exchange interactions; the energy for a certain Γ , including this effect of H_{SOC} , could be expressed as $E_{\Gamma} \pm c_{\Gamma}\lambda$, where λ is the coupling constant of H_{SOC} and $c_{\Gamma} = O(1)$ or $O(0.1)$. Accordingly, the modulations of the exchange interactions which come from the intermediate states for Γ are roughly given by $E_{\Gamma}/(E_{\Gamma} \pm c_{\Gamma}\lambda) \sim 1 \mp c_{\Gamma}(\lambda/E_{\Gamma})$. Since $\lambda = O(0.1 \text{ eV})$ in α -RuCl₃, we have $(\lambda/E_{\Gamma}) = O(0.1)$, and thus the corrections due to SOC are small for α -RuCl₃. From the above arguments, we conclude that our treatment, in which the effect of SOC on the coefficients of the exchange interactions is neglected, is sufficient for discussing the exchange interactions of α -RuCl₃ qualitatively.

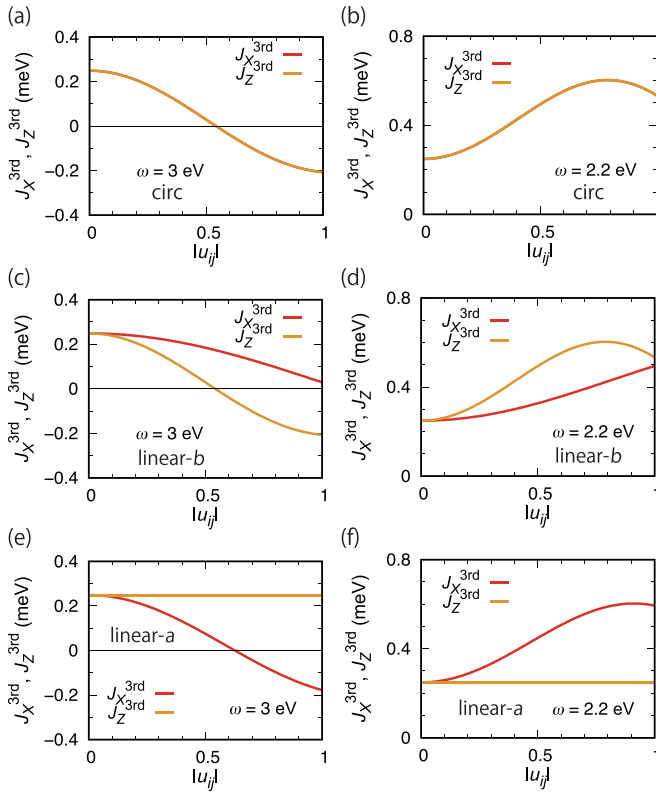


FIG. 13. The $|u_{ij}|$ dependences of J_{δ}^{3rd} in the third or fourth case of our model, in which $t_{3rd} = -40$ meV, with $\mathbf{E}_{\text{circ}}(t)$ [(a) and (b)], $\mathbf{E}_{\text{linear-b}}(t)$ [(c) and (d)], and $\mathbf{E}_{\text{linear-a}}(t)$ [(e) and (f)]. The value of ω is 3 eV in (a)–(c) and 2.2 eV in (d)–(f). In (a) and (b), $J_X^{3rd} = J_Y^{3rd} = J_Z^{3rd} = J_{3rd}$. The similar $|u_{ij}|$ dependences are obtained in the fifth case.

Next, we make some remarks about heating effects. Since the periodic driving field causes the system to heat up, it eventually approaches an infinite-temperature state [33]. However, there are intermediate times $t \lesssim \tau$ at which the periodically driven system can be approximately described by the Floquet Hamiltonian [4,5]. Since τ is roughly given by $\tau \approx T \exp(\omega/J_{\text{ex}})$ [5] and our parameters satisfy $\omega = O(1 \text{ eV})$ and $J_{\text{ex}} = \max(J_{\delta}, K_{\delta}, \Gamma_{\delta}, J_{\delta}^{3rd}) = O(10 \text{ meV})$, the intermediate times of our system may be sufficiently large. Note that because of these values of ω and J_{ex} , the correction to the Floquet Hamiltonian, the second term of Eq. (58), is negligible. Then, since our ω is nonresonant, the heating effect due to the doublon creation induced by the driving field is also negligible [22]. (Since this heating effect is non-negligible for resonant or nearly resonant ω , we have shown the results for some nonresonant ω 's in Secs. III B and IV B.) It should be noted that the effects of the doublon creation due to the driving field can be described by \bar{H}_{KE} in Eq. (55), and that they become negligible if ω is nonresonant in the sense that the denominator of Eq. (55) does not diverge [22]. (If ω is resonant or nearly resonant, \bar{H}_{KE} induces a non-negligible imaginary part, resulting in the heating effects [22].) Thus, we believe our results based on the Floquet Hamiltonian are meaningful as the properties of periodically driven α -RuCl₃.

We also remark on a property induced by the field of circularly polarized light. It has been shown for a single-

orbital Hubbard model driven by circularly polarized light [34,35] that when the light frequency is comparable with the Hubbard interaction, the effective Hamiltonian of the Mott insulator could acquire a spin scalar chirality, which is non-negligible compared with the antiferromagnetic Heisenberg interaction. Note that the spin scalar chirality terms come from the fourth-order perturbation processes in which the kinetic terms are treated as perturbation, whereas the exchange interactions come from the second-order ones. Although a similar mechanism might work in more complicated models, our rough estimate shown below indicates that such contributions may be negligible in our cases. Since the dominant Bessel functions appearing in the exchange interactions and the spin scalar chirality terms are $\mathcal{J}_0(u_{ij})$ and $\mathcal{J}_1(u_{ij})$, a ratio of J_{chi} , one of the spin scalar chirality terms, to J_{exch} , one of the exchange interactions, may be roughly given by $|J_{\text{chi}}/J_{\text{exch}}| \sim t^2 \mathcal{J}_1(u_{ij})^2 / (U_{\text{int}}|U_{\text{int}} - \omega|)$, where t is of the order of the hopping integrals and U_{int} is of the order of the on-site Coulomb interactions; in some cases of our analyses, our parameters correspond to $t = O(0.1 \text{ eV})$, $U_{\text{int}} = O(1 \text{ eV})$, and $|U_{\text{int}} - \omega| = O(0.1 \text{ eV})$. (Precisely speaking, our $|U_{\Gamma} - n\omega|$'s for any Γ and allowed n are larger than the hopping integrals.) In addition, since $\mathcal{J}_1(u_{ij})^2 = O(0.1)$, we have $|J_{\text{chi}}/J_{\text{ex}}| \sim 10^{-2}$. Although there is another contribution to the spin scalar chirality terms, J'_{chi} , it may be smaller than the above contribution because of an additional factor $|U_{\text{int}} - \omega|/\omega = O(10^{-1})$ [i.e., $|J'_{\text{chi}}/J_{\text{chi}}| \sim |U_{\text{int}} - \omega|/\omega = O(10^{-1})$]. Thus, we believe the spin scalar chirality terms are negligible and the results shown in Sec. IV B remain qualitatively unchanged.

We now address an experimental observation of our results. Controlling the exchange interactions via a light field, in principle, is achievable by performing pump-probe measurements. However, a strong light field is necessary because the ω 's considered in our study are high. For example, to realize the periodically driven α -RuCl₃ at $\omega = 2.2 \text{ eV}$ for $|u_{ij}| \sim 0.4$ or 0.6 , the amplitude of a light field, E_0 , should be $E_0 \sim 26$ or 39 MV cm^{-1} , respectively [for the relation between u_{ij} and E_0 , see Eq. (45)]; in the cases at $\omega = 1.8 \text{ eV}$ for $|u_{ij}| \sim 0.4$ or 0.6 , we have $E_0 \sim 21$ or 32 MV cm^{-1} , respectively. In these estimates, we have used $a_{\text{NN}} \sim 3.4 \times 10^{-8} \text{ cm}$, which corresponds to the average of the experimentally observed lengths of two nearest-neighbor bonds [36]. Then, the properties of the magnetic states could be observed by using, for example, neutron scattering measurements. Specifically, the changes in the competing magnetic states due to linearly polarized light could be detected as the evolution of short-range correlations characterized by the corresponding ordering vectors. Since a light field of the order of 10 MV cm^{-1} can be realized experimentally [37], we hope our main results, i.e., the changes in the exchange interactions, their bond anisotropy, and the competing magnetic states via linearly polarized light, will be observed by experiments.

Finally, we comment on several directions for further relevant research. First, our theory can be extended to the cases of α -RuCl₃ with both a light field and an external magnetic field and of other periodically driven Mott insulators on the honeycomb lattice (e.g., some Ir oxides). Our theory may be also useful for formulating a theory in the case on another lattice with strong SOC. The studies in these cases are contained in the possible research directions. Another research direction is

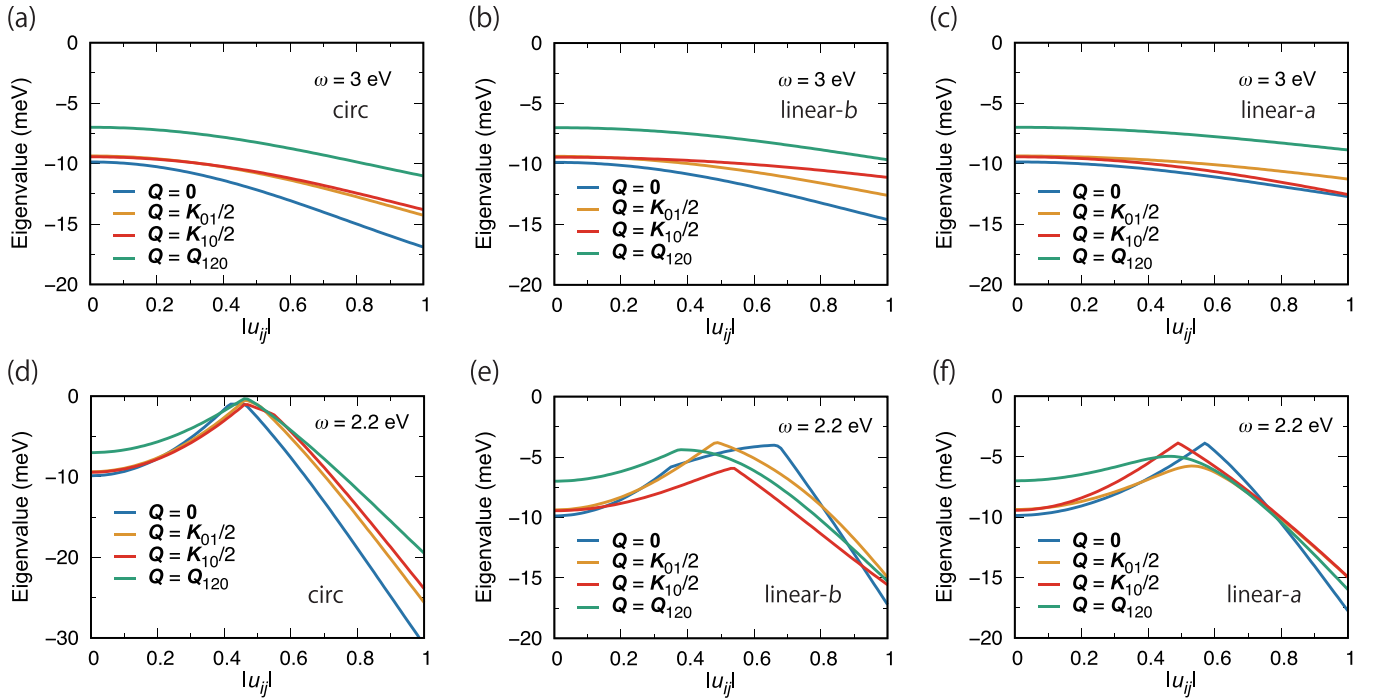


FIG. 14. The $|u_{ij}|$ dependences of the energies of the magnetic states for $\mathbf{Q} = \mathbf{0}$, $\mathbf{Q}_{ZZ-X}(=K_{01}/2)$, $\mathbf{Q}_{ZZ-Z}(=K_{10}/2)$, and \mathbf{Q}_{120} within the MFA in the fourth case of our model with $\mathbf{E}_{\text{circ}}(t)$ [(a) and (d)], $\mathbf{E}_{\text{linear-b}}(t)$ [(b) and (e)], and $\mathbf{E}_{\text{linear-a}}(t)$ [(c) and (f)]. The value of ω is 3 eV in (a)–(c) and 2.2 eV in (d)–(f). In this case, the bond-anisotropic nearest-neighbor hopping integrals and the third-neighbor one are considered.

to study a possibility of Kitaev spin liquids in a more elaborate method than the MFA. Such recent studies include Ref. [38]. In addition, our results may be useful for realizing a gapped

spin liquid, a toric code phase [39,40], because it could be stabilized in the presence of strong bond anisotropy of the exchange interactions. One of the possible situations might be

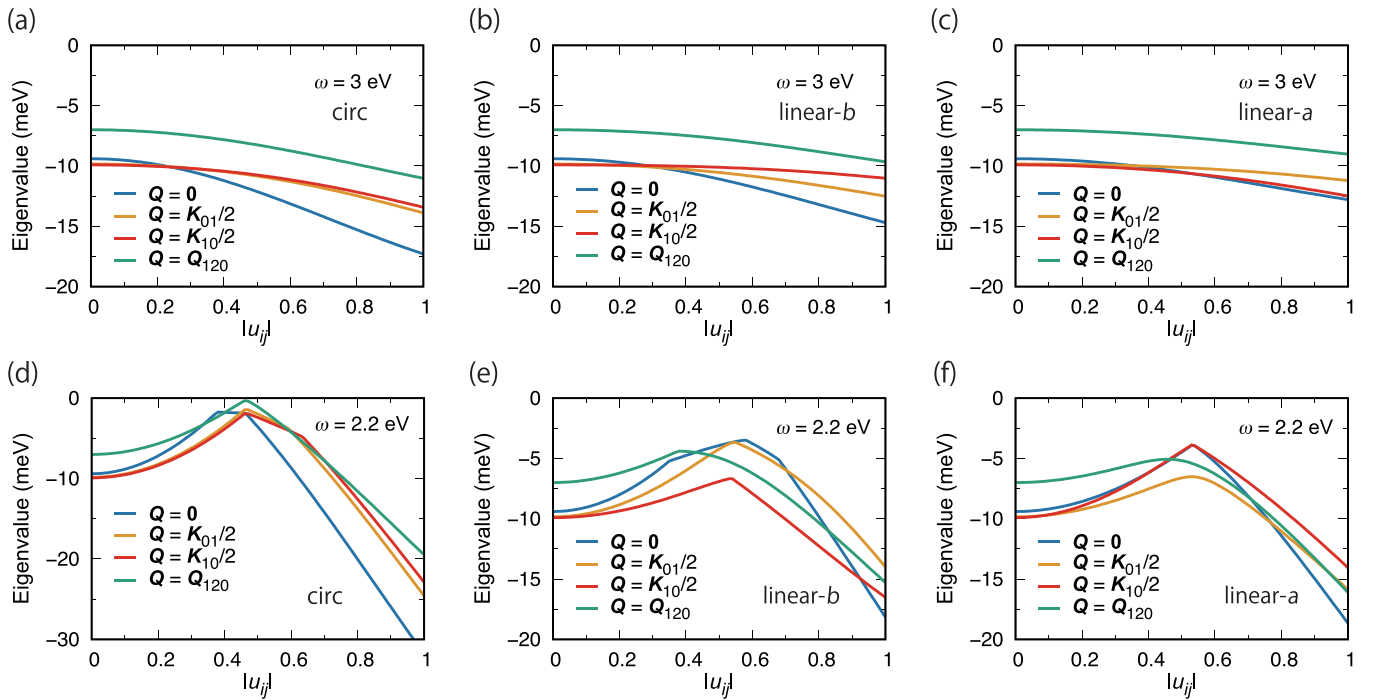


FIG. 15. The $|u_{ij}|$ dependences of the energies of the magnetic states for $\mathbf{Q} = \mathbf{0}$, $\mathbf{Q}_{ZZ-X}(=K_{01}/2)$, $\mathbf{Q}_{ZZ-Z}(=K_{10}/2)$, and \mathbf{Q}_{120} within the MFA in the fifth case of our model with $\mathbf{E}_{\text{circ}}(t)$ [(a) and (d)], $\mathbf{E}_{\text{linear-b}}(t)$ [(b) and (e)], and $\mathbf{E}_{\text{linear-a}}(t)$ [(c) and (f)]. The value of ω is 3 eV in (a)–(c) and 2.2 eV in (d)–(f). In this case, the bond-anisotropic nearest-neighbor hopping integrals and the third-neighbor one are considered; the difference between the parameters in the fourth and fifth cases is in the values of $t_{3\text{rd}}$.

α -RuCl₃ with both an in-plane magnetic field H_{ab} and a linearly polarized light field because a gapless spin liquid could be stabilized for α -RuCl₃ in the range of $7.5\text{T} < H_{ab} < 16\text{T}$ [41] and a linearly polarized light field could induce the strong bond anisotropy. Then, our results about the exchange interactions could be used to control magnetization dynamics and spintronics phenomena of Mott insulators with strong SOC because the key quantities to describe them are the exchange interactions [21,42]. Thus, the extensions to dynamical or transport properties are ones of the important future research directions. Another important future research direction is an extension to the case for small ω , at which the heating effects are no longer negligible.

VI. CONCLUSION

We have studied the magnetic properties of α -RuCl₃ driven by circularly or linearly polarized light. We showed that, as well as the magnitudes and signs of the exchange interactions, their bond anisotropy can be changed by tuning the amplitude and frequency of one of the fields of linearly polarized light. This is one of the characteristics of linearly polarized light because the bond anisotropy is not induced by circularly polarized light. Since the light-induced bond anisotropy can be used to change the ratios of J , K , and Γ for the Z bonds to those for the X or Y bonds, the honeycomb-network spin system could be transformed into weakly coupled zigzag or step chains for $\mathbf{E}_{\text{linear-}b}(t)$ or $\mathbf{E}_{\text{linear-}a}(t)$, respectively. We also showed that the $|u_{ij}|$ dependences of the exchange interactions obtained in the first case remain qualitatively unchanged except for the degeneracy lifting of the exchange interactions for the Z bonds and for the X and Y bonds. Then, we showed that the competing magnetic states can be changed only for linearly polarized light. Such a situation could be realized by using the strong field of the order of 10 MV cm^{-1} in pump-probe measurements. We also showed that the bond anisotropy of the nearest-neighbor hopping integrals and the third-neighbor hopping integral do not change qualitatively the results obtained in the first case of our model except for the stability of the zigzag states at $|u_{ij}| = 0$ and the degeneracy lifting of the magnetic states with $\mathbf{Q} = \mathbf{Q}_{ZZ-X}$ and \mathbf{Q}_{ZZ-Z} . We believe this paper is useful for further research of α -RuCl₃ and the relevant materials such as the honeycomb iridates and provides an important step towards a comprehensive understanding of magnetic properties of periodically driven Mott insulators with strong SOC.

ACKNOWLEDGMENTS

This work was supported by JST CREST Grant No. JPMJCR1901, JSPS KAKENHI Grants No. JP19K14664 and No. JP16K05459, and MEXT Q-LEAP Grant No. JP-MXS0118067426.

APPENDIX A: DERIVATION OF EQ. (44)

We calculate \bar{H}_{KE} 's for $\mathbf{A}(t) = \mathbf{A}_{\text{circ}}(t)$, $\mathbf{A}_{\text{linear-}b}(t)$, and $\mathbf{A}_{\text{linear-}a}(t)$. \bar{H}_{KE} is given by

$$\bar{H}_{\text{KE}} = \mathcal{P}_1 \frac{\omega}{2\pi} \int_0^{2\pi/\omega} dt H_{\text{KE}} \mathcal{P}_1$$

$$= \mathcal{P}_1 \frac{\omega}{2\pi} \int_0^{2\pi/\omega} dt \sum_{i,j} \sum_{a,b} \sum_{\sigma} t_{iajb} e^{-ie(\mathbf{R}_i - \mathbf{R}_j) \cdot \mathbf{A}(t)} \times c_{ia\sigma}^\dagger c_{jb\sigma} \mathcal{P}_1. \quad (\text{A1})$$

To perform the time integral, we rewrite the Peierls phase factor using Eqs. (6)–(8). For $\mathbf{A}(t) = \mathbf{A}_{\text{circ}}(t)$, we write it as follows [20]:

$$e^{-ie(\mathbf{R}_i - \mathbf{R}_j) \cdot \mathbf{A}(t)} = \begin{cases} e^{iu_{ij} \sin(\omega t + \frac{5\pi}{3})} & (X \text{ bonds}), \\ e^{iu_{ij} \sin(\omega t + \frac{\pi}{3})} & (Y \text{ bonds}), \\ e^{iu_{ij} \sin(\omega t + \pi)} & (Z \text{ bonds}), \end{cases} \quad (\text{A2})$$

where u_{ij} is defined in Eq. (45). Similarly, we obtain

$$e^{-ie(\mathbf{R}_i - \mathbf{R}_j) \cdot \mathbf{A}(t)} = \begin{cases} e^{i\frac{1}{2}u_{ij} \sin(\omega t - \frac{\pi}{2})} & (X \text{ or } Y \text{ bonds}), \\ e^{iu_{ij} \sin(\omega t + \frac{\pi}{2})} & (Z \text{ bonds}) \end{cases} \quad (\text{A3})$$

for $\mathbf{A}(t) = \mathbf{A}_{\text{linear-}b}(t)$, and

$$e^{-ie(\mathbf{R}_i - \mathbf{R}_j) \cdot \mathbf{A}(t)} = \begin{cases} e^{i\frac{\sqrt{3}}{2}u_{ij} \sin(\omega t + \frac{\pi}{2})} & (X \text{ bonds}), \\ e^{i\frac{\sqrt{3}}{2}u_{ij} \sin(\omega t - \frac{\pi}{2})} & (Y \text{ bonds}), \\ 1 & (Z \text{ bonds}) \end{cases} \quad (\text{A4})$$

for $\mathbf{A}(t) = \mathbf{A}_{\text{linear-}a}(t)$. By combining Eqs. (A2)–(A4) with Eq. (A1) and using the relations

$$e^{ix \sin \theta} = \sum_{n=-\infty}^{\infty} \mathcal{J}_n(x) e^{in\theta} \quad (\text{A5})$$

and

$$\frac{\omega}{2\pi} \int_0^{2\pi/\omega} dt e^{in\omega t} = \delta_{n,0}, \quad (\text{A6})$$

we obtain Eq. (44).

APPENDIX B: DERIVATION OF EQ. (50)

We solve Eq. (49). By integrating both sides and choosing for the initial state the state in which the lower-limit contributions of the integrals cancel each other out, we have

$$ie^{i(\bar{H}_{\text{KE}} + \bar{H}_{\text{int}})t} |\Psi_1\rangle_t = \int^t dt' e^{i(\bar{H}_{\text{KE}} + \bar{H}_{\text{int}})t'} H_{\text{KE}} |\Psi_0\rangle_{t'}. \quad (\text{B1})$$

Furthermore, since the time variation of $|\Psi_0\rangle_{t'}$ is slow, we could write Eq. (B1) as

$$ie^{i(\bar{H}_{\text{KE}} + \bar{H}_{\text{int}})t} |\Psi_1\rangle_t \approx \int^t dt' e^{i(\bar{H}_{\text{KE}} + \bar{H}_{\text{int}})t'} H_{\text{KE}} |\Psi_0\rangle_{t'}. \quad (\text{B2})$$

By combining Eq. (B2) with Eq. (5) and Eqs. (A2)–(A5) and performing the time integral, we obtain Eq. (50).

APPENDIX C: DERIVATION OF EQ. (63)

We calculate the possible terms of Eq. (60) for the Z bonds. The calculations consist of two steps.

First, we calculate $\langle i; \Gamma, g_\Gamma | T_{ij} | i \rangle$ for $T_{ij} = T_{ij}^Z$. Since

$$|i\rangle = \{|+\rangle_1 |+\rangle_2, |+\rangle_1 |-\rangle_2, |-\rangle_1 |+\rangle_2, |-\rangle_1 |-\rangle_2\}, \quad (\text{C1})$$

we calculate the finite terms of $\langle i; \Gamma, g_\Gamma | T_{12}^Z | i \rangle$; the contributions from $\langle i; \Gamma, g_\Gamma | T_{21}^Z | i \rangle$ to \bar{H}_{eff} can be taken into account

by multiplying those from $\langle i; \Gamma, g_{\Gamma} | T_{12}^Z | i \rangle$ by two. Using Eqs. (18), (19), and (61), we have

$$T_{12}^Z | +, + \rangle = \frac{1}{3} [(t_3 - t_1) c_{1d_{yz}\downarrow}^{\dagger} c_{1d_{xy}\uparrow}^{\dagger} - i(t_1 - t_3) c_{1d_{zx}\downarrow}^{\dagger} c_{1d_{xy}\uparrow}^{\dagger} + 2t_2 c_{1d_{yz}\downarrow}^{\dagger} c_{1d_{zx}\downarrow}^{\dagger} - it_2 c_{1d_{yz}\downarrow}^{\dagger} c_{1d_{xy}\uparrow}^{\dagger} - t_2 c_{1d_{zx}\downarrow}^{\dagger} c_{1d_{xy}\uparrow}^{\dagger}] | 0 \rangle, \quad (C2)$$

$$T_{12}^Z | -, - \rangle = \frac{1}{3} [(t_1 - t_3) c_{1d_{yz}\uparrow}^{\dagger} c_{1d_{xy}\downarrow}^{\dagger} - i(t_1 - t_3) c_{1d_{zx}\uparrow}^{\dagger} c_{1d_{xy}\downarrow}^{\dagger} + 2t_2 c_{1d_{yz}\uparrow}^{\dagger} c_{1d_{zx}\uparrow}^{\dagger} - it_2 c_{1d_{yz}\uparrow}^{\dagger} c_{1d_{xy}\downarrow}^{\dagger} + t_2 c_{1d_{zx}\uparrow}^{\dagger} c_{1d_{xy}\downarrow}^{\dagger}] | 0 \rangle, \quad (C3)$$

$$T_{12}^Z | +, - \rangle = \frac{1}{3} [-(t_1 - it_2) c_{1d_{yz}\uparrow}^{\dagger} c_{1d_{yz}\downarrow}^{\dagger} - (t_1 + it_2) c_{1d_{zx}\uparrow}^{\dagger} c_{1d_{zx}\downarrow}^{\dagger} - (it_1 + t_2) c_{1d_{yz}\uparrow}^{\dagger} c_{1d_{zx}\downarrow}^{\dagger} + (it_1 - t_2) c_{1d_{zx}\uparrow}^{\dagger} c_{1d_{yz}\downarrow}^{\dagger} - (t_1 - it_2) c_{1d_{yz}\uparrow}^{\dagger} c_{1d_{xy}\uparrow}^{\dagger} + (it_1 - t_2) c_{1d_{zx}\uparrow}^{\dagger} c_{1d_{xy}\uparrow}^{\dagger} - t_3 c_{1d_{yz}\downarrow}^{\dagger} c_{1d_{xy}\downarrow}^{\dagger} - it_3 c_{1d_{zx}\downarrow}^{\dagger} c_{1d_{xy}\downarrow}^{\dagger} - t_3 c_{1d_{xy}\uparrow}^{\dagger} c_{1d_{xy}\downarrow}^{\dagger}] | 0 \rangle, \quad (C4)$$

$$T_{12}^Z | -, + \rangle = \frac{1}{3} [(t_1 + it_2) c_{1d_{yz}\uparrow}^{\dagger} c_{1d_{yz}\downarrow}^{\dagger} + (t_1 - it_2) c_{1d_{zx}\uparrow}^{\dagger} c_{1d_{zx}\downarrow}^{\dagger} + (it_1 + t_2) c_{1d_{yz}\uparrow}^{\dagger} c_{1d_{zx}\downarrow}^{\dagger} - (it_1 - t_2) c_{1d_{zx}\uparrow}^{\dagger} c_{1d_{yz}\downarrow}^{\dagger} + (t_1 + it_2) c_{1d_{yz}\downarrow}^{\dagger} c_{1d_{xy}\downarrow}^{\dagger} + (it_1 + t_2) c_{1d_{zx}\downarrow}^{\dagger} c_{1d_{xy}\downarrow}^{\dagger} + t_3 c_{1d_{yz}\uparrow}^{\dagger} c_{1d_{xy}\uparrow}^{\dagger} - it_3 c_{1d_{zx}\uparrow}^{\dagger} c_{1d_{xy}\uparrow}^{\dagger} + t_3 c_{1d_{xy}\uparrow}^{\dagger} c_{1d_{xy}\downarrow}^{\dagger}] | 0 \rangle. \quad (C5)$$

By using Eqs. (C2)–(C5) and Eqs. (26)–(40), we can calculate $\langle i; \Gamma, g_{\Gamma} | T_{12}^Z | i \rangle$'s; as a result, the finite terms are given by

$$\begin{aligned} \langle i; A_1 | T_{12}^Z | +, - \rangle &= -\langle i; A_1 | T_{12}^Z | -, + \rangle \\ &= -\frac{1}{3\sqrt{3}}(2t_1 + t_3), \end{aligned} \quad (C6)$$

$$\begin{aligned} \langle i; E, u | T_{12}^Z | +, - \rangle &= -\langle i; E, u | T_{12}^Z | -, + \rangle \\ &= -\frac{2}{3\sqrt{6}}(t_1 - t_3), \end{aligned} \quad (C7)$$

$$\langle i; E, v | T_{12}^Z | +, - \rangle = \langle i; E, v | T_{12}^Z | -, + \rangle = \frac{2}{3\sqrt{2}}it_2, \quad (C8)$$

$$\langle i; T_1, \alpha_+ | T_{12}^Z | -, - \rangle = \langle i; T_1, \alpha_- | T_{12}^Z | +, + \rangle = \frac{2}{3}t_2, \quad (C9)$$

$$\langle i; T_1, \alpha | T_{12}^Z | +, - \rangle = -\langle i; T_1, \alpha | T_{12}^Z | -, + \rangle = -\frac{2}{3\sqrt{2}}it_1, \quad (C10)$$

$$\langle i; T_2, \alpha | T_{12}^Z | +, - \rangle = -\langle i; T_2, \alpha | T_{12}^Z | -, + \rangle = -\frac{2}{3\sqrt{2}}t_2, \quad (C11)$$

$$\langle i; T_1, \beta_+ | T_{12}^Z | +, - \rangle = \frac{1}{3}(it_1 - t_2), \quad (C12)$$

$$\langle i; T_1, \beta_+ | T_{12}^Z | -, + \rangle = \langle i; T_1, \beta_- | T_{12}^Z | +, - \rangle = -\frac{i}{3}t_3, \quad (C13)$$

$$\langle i; T_1, \beta_- | T_{12}^Z | -, + \rangle = \frac{1}{3}(it_1 + t_2), \quad (C14)$$

$$\langle i; T_1, \beta | T_{12}^Z | +, + \rangle = -\frac{1}{3\sqrt{2}}[i(t_1 - t_3) + t_2], \quad (C15)$$

$$\langle i; T_1, \beta | T_{12}^Z | -, - \rangle = -\frac{1}{3\sqrt{2}}[i(t_1 - t_3) - t_2], \quad (C16)$$

$$\langle i; T_2, \beta | T_{12}^Z | +, + \rangle = \frac{1}{3\sqrt{2}}[i(t_1 - t_3) + t_2], \quad (C17)$$

$$\langle i; T_2, \beta | T_{12}^Z | -, - \rangle = -\frac{1}{3\sqrt{2}}[i(t_1 - t_3) - t_2], \quad (C18)$$

$$\langle i; T_1, \gamma_+ | T_{12}^Z | +, - \rangle = \frac{1}{3}(t_1 - it_2), \quad (C19)$$

$$\langle i; T_1, \gamma_+ | T_{12}^Z | -, + \rangle = -\langle i; T_1, \gamma_- | T_{12}^Z | +, - \rangle = -\frac{1}{3}t_3, \quad (C20)$$

$$\langle i; T_1, \gamma_- | T_{12}^Z | -, + \rangle = -\frac{1}{3}(t_1 + it_2), \quad (C21)$$

$$\langle i; T_1, \gamma | T_{12}^Z | +, + \rangle = \frac{1}{3\sqrt{2}}[(t_1 - t_3) + it_2], \quad (C22)$$

$$\langle i; T_1, \gamma | T_{12}^Z | -, - \rangle = -\frac{1}{3\sqrt{2}}[(t_1 - t_3) - it_2], \quad (C23)$$

$$\langle i; T_2, \gamma | T_{12}^Z | +, + \rangle = \frac{1}{3\sqrt{2}}[(t_1 - t_3) + it_2], \quad (C24)$$

$$\langle i; T_2, \gamma | T_{12}^Z | -, - \rangle = \frac{1}{3\sqrt{2}}[(t_1 - t_3) - it_2], \quad (C25)$$

and the others are zero.

Then, we express Eq. (60) for the Z bonds in terms of the exchange interactions. By combining Eqs. (C6)–(C25) and Eqs. (22)–(25) with Eq. (60), we can write \tilde{H}_{eff}^Z for the Z bonds, \tilde{H}_{eff}^Z , as follows:

$$\tilde{H}_{\text{eff}}^Z = H_{A_1} + H_E + H_{T_1} + H_{T_2}, \quad (C26)$$

where

$$H_{A_1} = \sum_{(i,j)_Z} \sum_{n=-\infty}^{\infty} \frac{4(2t_1 + t_3)^2 \mathcal{J}_n(u_{ij}^Z)^2}{27(U + 2J' - n\omega)} \mathbf{S}_i \cdot \mathbf{S}_j, \quad (C27)$$

$$\begin{aligned} H_E &= \sum_{(i,j)_Z} \sum_{n=-\infty}^{\infty} \frac{8\mathcal{J}_n(u_{ij}^Z)^2}{27(U - J' - n\omega)} \\ &\times \{ [(t_1 - t_3)^2 - 3t_2^2] \mathbf{S}_i \cdot \mathbf{S}_j + 6t_2^2 S_i^z S_j^z \}, \end{aligned} \quad (C28)$$

$$\begin{aligned} H_{T_1} &= \sum_{(i,j)_Z} \sum_{n=-\infty}^{\infty} \frac{4\mathcal{J}_n(u_{ij}^Z)^2}{9(U' - J_H - n\omega)} \\ &\times \{ -[(t_1 - t_3)^2 + t_2^2 - 2t_1^2 - 4t_1 t_3] \mathbf{S}_i \cdot \mathbf{S}_j \\ &+ [(t_1 - t_3)^2 + t_2^2] (S_i^y S_j^y + S_i^x S_j^x) \\ &+ 2t_2(t_1 - t_3) (S_i^x S_j^y + S_i^y S_j^x) \\ &+ 2[(t_1^2 + t_2^2 + t_3^2) - 2t_2^2 - 2t_1 t_3] S_i^z S_j^z \}, \end{aligned} \quad (C29)$$

$$\begin{aligned} H_{T_2} &= \sum_{(i,j)_Z} \sum_{n=-\infty}^{\infty} \frac{4\mathcal{J}_n(u_{ij}^Z)^2}{9(U' + J_H - n\omega)} \\ &\times \{ [(t_1 - t_3)^2 + t_2^2] (S_i^x S_j^x + S_i^y S_j^y) \\ &- 2t_2(t_1 - t_3) (S_i^x S_j^y + S_i^y S_j^x) \} \end{aligned}$$

$$- [(t_1 - t_3)^2 - t_2^2] \mathbf{S}_i \cdot \mathbf{S}_j. \quad (\text{C30})$$

In deriving these equations, we have used the relations of operators in the $j_{\text{eff}} = 1/2$ subspace [e.g., $|- , + \rangle \langle - , + | = (\frac{1}{2} - S_1^z)(\frac{1}{2} + S_2^z)$ and $|- , + \rangle \langle + , - | = S_1^- S_2^+$] and omitted the constant terms. By using the identity $S_i^x S_j^x + S_i^y S_j^y = \mathbf{S}_i \cdot \mathbf{S}_j - S_i^z S_j^z$, we can rewrite Eqs. (C29) and (C30). A combination of the resultant equations and Eqs. (C26)–(C28) gives Eq. (63).

APPENDIX D: ESTIMATES OF THE VALUES OF J_δ^{3rd} AND K_δ^{3rd}

We estimate J_δ^{3rd} and K_δ^{3rd} at $E_0 = 0$ in two cases. In the following estimation, we calculate their values for the Z_3 bonds (Fig. 1) because the bond anisotropy of the third-neighbor hopping integrals is weak [13]; the values of the third-neighbor hopping integrals used below are consistent with those of Ref. [13]. Then, we set $J' = J_H$, $U' = U - 2J_H$, $U = 3 \text{ eV}$, and $J_H = 0.5 \text{ eV}$.

If we consider only $t_{3\text{rd}}$, the intraorbital hopping integral of the d_{xy} orbital, among the third-neighbor hopping integrals, J_Z^{3rd} and K_Z^{3rd} at $E_0 = 0$ are given by

$$J_Z^{\text{3rd}} = \frac{4t_{3\text{rd}}^2}{27(U + 2J_H)} + \frac{8t_{3\text{rd}}^2}{27(U - J_H)} \quad (\text{D1})$$

and

$$K_Z^{\text{3rd}} = \frac{4}{9} t_{3\text{rd}}^2 \left(\frac{1}{U - 3J_H} - \frac{1}{U - J_H} \right), \quad (\text{D2})$$

respectively. If we set $t_{3\text{rd}} \sim -40 \text{ meV}$, we have $J_Z^{\text{3rd}} \sim 0.25 \text{ meV}$ and $K_Z^{\text{3rd}} \sim 0.19 \text{ meV}$.

Next, we consider not only $t_{3\text{rd}}$, but also two additional terms of third-neighbor hopping integrals, $t'_{3\text{rd}}$ and $t''_{3\text{rd}}$. Here $t'_{3\text{rd}}$ represents the intraorbital hopping integral of the d_{yz} or d_{zx} orbital and $t''_{3\text{rd}}$ represents the interorbital hopping integral between these orbitals. Then, we can write J_Z^{3rd} and K_Z^{3rd} at $E_0 = 0$ as follows:

$$J_Z^{\text{3rd}} = \frac{4(2t'_{3\text{rd}} + t_{3\text{rd}})^2}{27(U + 2J_H)} + \frac{8(t'_{3\text{rd}} - t_{3\text{rd}})^2}{27(U - J_H)} + \frac{8t'_{3\text{rd}}(t'_{3\text{rd}} + 2t_{3\text{rd}})}{9(U - 3J_H)}, \quad (\text{D3})$$

$$K_Z^{\text{3rd}} = \frac{4}{9} [(t'_{3\text{rd}} - t_{3\text{rd}})^2 - 3(t''_{3\text{rd}})^2] \times \left(\frac{1}{U - 3J_H} - \frac{1}{U - J_H} \right). \quad (\text{D4})$$

Setting $t_{3\text{rd}} \sim -40 \text{ meV}$, $t'_{3\text{rd}} \sim -8 \text{ meV}$, and $t''_{3\text{rd}} \sim -7 \text{ meV}$, we have $J_Z^{\text{3rd}} \sim 0.65 \text{ meV}$ and $K_Z^{\text{3rd}} \sim 0.1 \text{ meV}$.

Comparing the estimated values in the above two cases, we see J_Z^{3rd} and K_Z^{3rd} are underestimated and overestimated, respectively, if we consider only $t_{3\text{rd}}$ among the third-neighbor hopping integrals. Since K_δ^{3rd} is much smaller than J_δ^{3rd} even in a more realistic situation [13], we consider only J_δ^{3rd} and neglect K_δ^{3rd} in our analyses.

APPENDIX E: DERIVATION OF EQ. (88)

We rewrite Eq. (83) using Eqs. (86) and (87). First, we can rewrite the terms of J_δ 's as

$$\begin{aligned} & \sum_{(i,j)} J_\delta \langle \mathbf{S}_i \rangle \cdot \langle \mathbf{S}_j \rangle \\ &= \frac{1}{2} \sum_{i=1}^{N/2} \sum_{j=1}^{z_{\text{NN}}} J_\delta \langle \mathbf{S}_i \rangle \cdot \langle \mathbf{S}_j \rangle + \frac{1}{2} \sum_{j=1}^{N/2} \sum_{i=1}^{z_{\text{NN}}} J_\delta \langle \mathbf{S}_i \rangle \cdot \langle \mathbf{S}_j \rangle \\ &= \sum_{\mathbf{q}} \sum_{\mu=x,y,z} [J_1(\mathbf{q}) \langle S_{-qA}^\mu \rangle \langle S_{qB}^\mu \rangle + J_1(\mathbf{q})^* \langle S_{-qB}^\mu \rangle \langle S_{qA}^\mu \rangle], \end{aligned} \quad (\text{E1})$$

where

$$\begin{aligned} J_1(\mathbf{q}) &= \sum_{j=1}^{z_{\text{NN}}} \frac{J_\delta}{2} e^{-iq \cdot (\mathbf{R}_i - \mathbf{R}_j)} \\ &= \frac{J_X}{2} e^{-i\frac{q_x}{2} + i\frac{\sqrt{3}}{2}q_y} + \frac{J_Y}{2} e^{-i\frac{q_x}{2} - i\frac{\sqrt{3}}{2}q_y} + \frac{J_Z}{2} e^{iq_x}, \end{aligned} \quad (\text{E2})$$

and z_{NN} denotes the number of nearest-neighbor sites at a certain site on the honeycomb lattice. In Eq. (E2), the first, second, and third terms correspond to the contributions from the X, Y, and Z bonds (Fig. 1), respectively. Similarly, we can express the other terms as follows:

$$\begin{aligned} & \sum_{(i,j)} K_\delta \langle S_i^y \rangle \langle S_j^y \rangle \\ &= \sum_{\mathbf{q}} [K_x(\mathbf{q}) \langle S_{-qA}^x \rangle \langle S_{qB}^x \rangle + K_y(\mathbf{q}) \langle S_{-qA}^y \rangle \langle S_{qB}^y \rangle \\ & \quad + K_z(\mathbf{q}) \langle S_{-qA}^z \rangle \langle S_{qB}^z \rangle] \\ & \quad + \sum_{\mathbf{q}} [K_x(\mathbf{q})^* \langle S_{-qB}^x \rangle \langle S_{qA}^x \rangle + K_y(\mathbf{q})^* \langle S_{-qB}^y \rangle \langle S_{qA}^y \rangle \\ & \quad + K_z(\mathbf{q})^* \langle S_{-qB}^z \rangle \langle S_{qA}^z \rangle], \end{aligned} \quad (\text{E3})$$

$$\begin{aligned} & \sum_{(i,j)} \Gamma_\delta (\langle S_i^\alpha \rangle \langle S_j^\beta \rangle + \langle S_i^\beta \rangle \langle S_j^\alpha \rangle) \\ &= \sum_{\mathbf{q}} [\Gamma_x(\mathbf{q}) (\langle S_{-qA}^y \rangle \langle S_{qB}^z \rangle + \langle S_{-qA}^z \rangle \langle S_{qB}^y \rangle) \\ & \quad + \Gamma_y(\mathbf{q}) (\langle S_{-qA}^z \rangle \langle S_{qB}^x \rangle + \langle S_{-qA}^x \rangle \langle S_{qB}^z \rangle) \\ & \quad + \Gamma_z(\mathbf{q}) (\langle S_{-qA}^x \rangle \langle S_{qB}^y \rangle + \langle S_{-qA}^y \rangle \langle S_{qB}^x \rangle)] \\ & \quad + \sum_{\mathbf{q}} [\Gamma_x(\mathbf{q})^* (\langle S_{-qB}^y \rangle \langle S_{qA}^z \rangle + \langle S_{-qB}^z \rangle \langle S_{qA}^y \rangle) \\ & \quad + \Gamma_y(\mathbf{q})^* (\langle S_{-qB}^z \rangle \langle S_{qA}^x \rangle + \langle S_{-qB}^x \rangle \langle S_{qA}^z \rangle) \\ & \quad + \Gamma_z(\mathbf{q})^* (\langle S_{-qB}^x \rangle \langle S_{qA}^y \rangle + \langle S_{-qB}^y \rangle \langle S_{qA}^x \rangle)], \end{aligned} \quad (\text{E4})$$

$$\begin{aligned} & \sum_{\langle\langle(i,j)\rangle\rangle} J_\delta^{\text{3rd}} \langle \mathbf{S}_i \rangle \cdot \langle \mathbf{S}_j \rangle \\ &= \sum_{\mathbf{q}} \sum_{\mu=x,y,z} [J_3(\mathbf{q}) \langle S_{-qA}^\mu \rangle \langle S_{qB}^\mu \rangle + J_3(\mathbf{q})^* \langle S_{-qB}^\mu \rangle \langle S_{qA}^\mu \rangle], \end{aligned} \quad (\text{E5})$$

where $K_\mu(\mathbf{q})$'s and $\Gamma_\mu(\mathbf{q})$'s have been defined in Eqs. (91)–(96), and $J_3(\mathbf{q})$ is given by

$$J_3(\mathbf{q}) = \frac{J_X^{\text{3rd}}}{2} e^{iq_x - i\sqrt{3}q_y} + \frac{J_Y^{\text{3rd}}}{2} e^{iq_x + i\sqrt{3}q_y} + \frac{J_Z^{\text{3rd}}}{2} e^{-2iq_x}. \quad (\text{E6})$$

By combining Eqs. (E1)–(E6) and setting $J(\mathbf{q}) = J_1(\mathbf{q}) + J_3(\mathbf{q})$, we obtain Eq. (88).

APPENDIX F: SOME REMARKS ON MOMENTUM

We remark on momentum in the case of the honeycomb lattice. The remarks are about its expression and the reciprocal lattice vector with the periodic boundary condition. In the case of the honeycomb lattice (Fig. 1) a set of primitive vectors, \mathbf{a}_1 and \mathbf{a}_2 , can be written as

$$\mathbf{a}_1 = {}^t \left(\frac{\sqrt{3}}{2} a_{2\text{nd}} \quad \frac{1}{2} a_{2\text{nd}} \right) = {}^t \left(\frac{3}{2} \quad \frac{\sqrt{3}}{2} \right), \quad (\text{F1})$$

$$\mathbf{a}_2 = {}^t (0 \quad a_{2\text{nd}}) = {}^t (0 \quad \sqrt{3}), \quad (\text{F2})$$

and thus the primitive vectors for the reciprocal lattice, \mathbf{b}_1 and \mathbf{b}_2 , are given by

$$\mathbf{b}_1 = {}^t \left(\frac{4\pi}{3} \quad 0 \right), \quad (\text{F3})$$

$$\mathbf{b}_2 = {}^t \left(-\frac{2\pi}{3} \quad \frac{2\pi}{\sqrt{3}} \right). \quad (\text{F4})$$

(As described in the caption of Fig. 1, we can represent the honeycomb lattice as a triangular Bravais lattice with a two-

sublattice structure [23].) By imposing the periodic boundary condition [23], we can express momentum \mathbf{q} as

$$\mathbf{q} = \frac{l_1}{N_1} \mathbf{b}_1 + \frac{l_2}{N_2} \mathbf{b}_2, \quad (\text{F5})$$

where the integers l_1 and l_2 satisfy $0 \leq l_1 < N_1$ and $0 \leq l_2 < N_2$ with $N_1 N_2 = N$. As described in Sec. IV B, we set $N_1 = N_2 = 120$ in our analyses. The values of l_1 and l_2 for the magnetic states considered in Sec. IV B are given as follows: for $\mathbf{q} = \mathbf{Q}_{ZZ-X}$ $l_1 = N_1/4$ and $l_2 = N_1/2$; for $\mathbf{q} = \mathbf{Q}_{ZZ-Z}$ $l_1 = N_1/2$ and $l_2 = 0$; and for $\mathbf{q} = \mathbf{Q}_{120}$ $l_1 = l_2 = (2N_1/3)$. Then, the reciprocal lattice vector \mathbf{K} can be written as

$$\mathbf{K} = {}^t (K_x \quad K_y) = m_1 \mathbf{b}_1 + m_2 \mathbf{b}_2, \quad (\text{F6})$$

where

$$K_x = \frac{2\pi}{3} (2m_1 - m_2), \quad K_y = \frac{2\pi}{\sqrt{3}} m_2, \quad (\text{F7})$$

and m_1 and m_2 are integers. From these equations, we see that \mathbf{K} for $(m_1, m_2) = (0, 1)$, \mathbf{K}_{01} , equals $2\mathbf{Q}_{ZZ-X}$, and that \mathbf{K} for $(m_1, m_2) = (1, 0)$, \mathbf{K}_{10} , equals $2\mathbf{Q}_{ZZ-Z}$. Namely, we have

$$\mathbf{Q}_{ZZ-X} = \frac{\mathbf{K}_{01}}{2}, \quad (\text{F8})$$

$$\mathbf{Q}_{ZZ-Z} = \frac{\mathbf{K}_{10}}{2}. \quad (\text{F9})$$

In contrast to \mathbf{Q}_{ZZ-X} and \mathbf{Q}_{ZZ-Z} , \mathbf{Q}_{120} is not equal to $\mathbf{K}/2$ for any allowed m_1 and m_2 .

-
- [1] J. H. Shirley, Solution of the Schrödinger equation with a Hamiltonian periodic in time, *Phys. Rev.* **138**, B979 (1965).
- [2] H. Sambe, Steady states and quasienergies of a quantum-mechanical system in an oscillating field, *Phys. Rev. A* **7**, 2203 (1973).
- [3] M. Bukov, L. D'Alessio, and A. Polkovnikov, Universal high-frequency behavior of periodically driven systems: From dynamical stabilization to Floquet engineering, *Adv. Phys.* **64**, 139 (2015).
- [4] D. A. Abanin, W. De Roeck, and F. Huveneers, Exponentially Slow Heating in Periodically Driven Many-Body Systems, *Phys. Rev. Lett.* **115**, 256803 (2015).
- [5] T. Kuwahara, T. Mori, and K. Saito, Floquet-Magnus theory and generic transient dynamics in periodically driven many-body quantum systems, *Ann. Phys. (Amsterdam, Neth.)* **367**, 96 (2016).
- [6] J. H. Mentink, K. Balzer, and M. Eckstein, Ultrafast and reversible control of the exchange interaction in Mott insulators, *Nat. Commun.* **6**, 6708 (2015).
- [7] B. J. Kim, H. Jin, S. J. Moon, J.-Y. Kim, B.-G. Park, C. S. Leem, J. Yu, T. W. Noh, C. Kim, S.-J. Oh, J.-H. Park, V. Durairaj, G. Cao, and E. Rotenberg, Novel $J_{\text{eff}} = 1/2$ Mott State Induced by Relativistic Spin-Orbit Coupling in Sr_2IrO_4 , *Phys. Rev. Lett.* **101**, 076402 (2008).
- [8] W. Witczak-Krempa, G. Chen, Y. B. Kim, and L. Balents, Correlated quantum phenomena in the strong spin-orbit regime, *Annu. Rev. Condens. Matter Phys.* **5**, 57 (2014).
- [9] T. Takayama, J. Chaloupka, A. Smerald, G. Khaliullin, and H. Takagi, Spin-orbit-entangled electronic phases in $4d$ and $5d$ transition-metal compounds, *J. Phys. Soc. Jpn.* **90**, 062001 (2021).
- [10] G. Jackeli and G. Khaliullin, Mott Insulators in the Strong Spin-Orbit Coupling Limit: From Heisenberg to a Quantum Compass and Kitaev Models, *Phys. Rev. Lett.* **102**, 017205 (2009).
- [11] J. Chaloupka, G. Jackeli, and G. Khaliullin, Kitaev-Heisenberg Model on a Honeycomb Lattice: Possible Exotic Phases in Iridium Oxides A_2IrO_3 , *Phys. Rev. Lett.* **105**, 027204 (2010).
- [12] J. G. Rau, E. K.-H. Lee, and H.-Y. Kee, Generic Spin Model for the Honeycomb Iridates beyond the Kitaev Limit, *Phys. Rev. Lett.* **112**, 077204 (2014).
- [13] S. M. Winter, Y. Li, H. O. Jeschke, and R. Valentí, Challenges in design of Kitaev materials: Magnetic interactions from competing energy scales, *Phys. Rev. B* **93**, 214431 (2016).
- [14] N. Arakawa, Vector chirality for effective total momentum J_{eff} in a nonfrustrated Mott insulator: Effects of strong spin-orbit coupling and broken inversion symmetry, *Phys. Rev. B* **94**, 174416 (2016).
- [15] J. G. Rau and H.-Y. Kee, Trigonal distortion in the honeycomb iridates: Proximity of zigzag and spiral phases in Na_2IrO_3 , [arXiv:1408.4811](https://arxiv.org/abs/1408.4811).
- [16] J. Chaloupka and G. Khaliullin, Hidden symmetries of the extended Kitaev-Heisenberg model: Implications for the honeycomb-lattice iridates A_2IrO_3 , *Phys. Rev. B* **92**, 024413 (2015).

- [17] L. Janssen, E. C. Andrade, and M. Vojta, Magnetization processes of zigzag states on the honeycomb lattice: Identifying spin models for α - RuCl_3 and Na_2IrO_3 , *Phys. Rev. B* **96**, 064430 (2017).
- [18] J. Wang, B. Normand, and Z.-X. Liu, One Proximate Kitaev Spin Liquid in the K - J - Γ Model on the Honeycomb Lattice, *Phys. Rev. Lett.* **123**, 197201 (2019).
- [19] J. Rusnačko, D. Gotfryd, and J. Chaloupka, Kitaev-like honeycomb magnets: Global phase behavior and emergent effective models, *Phys. Rev. B* **99**, 064425 (2019).
- [20] N. Arakawa and K. Yonemitsu, Floquet engineering of Mott insulators with strong spin-orbit coupling, *Phys. Rev. B* **103**, L100408 (2021).
- [21] A. Kirilyuk, A. V. Kimel, and T. Rasing, Ultrafast optical manipulation of magnetic order, *Rev. Mod. Phys.* **82**, 2731 (2010).
- [22] K. Hejazi, J. Liu, and L. Balents, Floquet spin and spin-orbital Hamiltonians and doublon-holon generations in periodically driven Mott insulators, *Phys. Rev. B* **99**, 205111 (2019).
- [23] N. W. Ashcroft and N. D. Mermin, *Solid State Physics* (Thomson Learning Inc., USA, 1976).
- [24] J. Kanamori, Electron correlation and ferromagnetism of transition metals, *Prog. Theor. Phys.* **30**, 275 (1963).
- [25] K. W. Plumb, J. P. Clancy, L. J. Sandilands, V. V. Shankar, Y. F. Hu, K. S. Burch, H.-Y. Kee, and Y.-J. Kim, α - RuCl_3 : A spin-orbit assisted Mott insulator on a honeycomb lattice, *Phys. Rev. B* **90**, 041112(R) (2014).
- [26] H.-S. Kim, V. Shankar V., A. Catuneanu, and H.-Y. Kee, Kitaev magnetism in honeycomb RuCl_3 with intermediate spin-orbit coupling, *Phys. Rev. B* **91**, 241110(R) (2015).
- [27] S. Ishihara, T. Hatakeyama, and S. Maekawa, Magnetic ordering, orbital ordering and resonant X-ray scattering in perovskite titanates, *Phys. Rev. B* **65**, 064442 (2002).
- [28] J. M. Luttinger and L. Tisza, Theory of dipole interaction in crystals, *Phys. Rev.* **70**, 954 (1946).
- [29] J. M. Luttinger, A note on the ground state in antiferromagnetics, *Phys. Rev.* **81**, 1015 (1951).
- [30] For the analysis in the region surrounded by the dashed white line in Fig. 2(a) of Ref. [12], the authors imposed an additional restriction.
- [31] H. Suzuki, H. Liu, J. Bertinshaw, K. Ueda, H. Kim, S. Laha, D. Weber, Z. Yang, L. Wang, H. Takahashi, K. Fursich, M. Minola, B. V. Lotsch, B. J. Kim, H. Yavass, M. Daghofer, J. Chaloupka, G. Khaliullin, H. Gretarsson, and B. Keimer, Proximate ferromagnetic state in the Kitaev model material α - RuCl_3 , *Nat. Commun.* **12**, 4512 (2021).
- [32] J. A. Sears, L. E. Chern, S. Kim, P. J. Bercier, S. Francoual, Y. B. Kim, and Y.-J. Kim, Ferromagnetic Kitaev interaction and the origin of large magnetic anisotropy in α - RuCl_3 , *Nat. Phys.* **16**, 837 (2020).
- [33] L. D'Alessio and M. Rigol, Long-time Behavior of Isolated Periodically Driven Interacting Lattice Systems, *Phys. Rev. X* **4**, 041048 (2014).
- [34] M. Claassen, H.-C. Jiang, B. Moritz, and T. P. Devereaux, Dynamical time-reversal symmetry breaking and photo-induced chiral spin liquids in frustrated Mott insulators, *Nat. Commun.* **8**, 1192 (2017).
- [35] S. Kitamura, T. Oka, and H. Aoki, Probing and controlling spin chirality in Mott insulators by circularly polarized laser, *Phys. Rev. B* **96**, 014406 (2017).
- [36] R. D. Johnson, S. C. Williams, A. A. Haghighirad, J. Singleton, V. Zapf, P. Manuel, I. I. Mazin, Y. Li, H. O. Jeschke, R. Valentí, and R. Coldea, Monoclinic crystal structure of α - RuCl_3 and the zigzag antiferromagnetic ground state, *Phys. Rev. B* **92**, 235119 (2015).
- [37] Y. Kawakami, H. Itoh, K. Yonemitsu, and S. Iwai, Strong light-field effects driven by nearly single-cycle 7 fs light-field in correlated organic conductors, *J. Phys. B: At. Mol. Opt. Phys.* **51**, 174005 (2018).
- [38] A. Sriram and M. Claassen, Light-Induced Control of Magnetic Phases in Kitaev Quantum Magnets, [arXiv:2105.01062](https://arxiv.org/abs/2105.01062).
- [39] A. Kitaev, Anyons in an exactly solved model and beyond, *Ann. Phys.* **321**, 2 (2006).
- [40] M. O. Takahashi, M. G. Yamada, D. Takikawa, T. Mizushima, and S. Fujimoto, Topological nematic phase transition in Kitaev magnets under applied magnetic fields, *Phys. Rev. Res.* **3**, 023189 (2021).
- [41] J. Zheng, K. Ran, T. Li, J. Wang, P. Wang, B. Liu, Z.-X. Liu, B. Normand, J. Wen, and W. Yu, Gapless Spin Excitations in the Field-Induced Quantum Spin Liquid Phase of α - RuCl_3 , *Phys. Rev. Lett.* **119**, 227208 (2017).
- [42] I. Žutić, J. Fabian, and S. D. Sarma, Spintronics: Fundamentals and applications, *Rev. Mod. Phys.* **76**, 323 (2004).